

# Conformal symmetry breaking and self-similar spirals

## *Jacob Bernoulli's Spira Mirabilis set free*

Jemal Guven

*Instituto de Ciencias Nucleares  
Universidad Nacional Autónoma de México  
Apdo. Postal 70-543, 04510 México, DF, MEXICO*

### Abstract

Self-similar curves are shown to arise naturally as tension-free stationary states of conformally invariant energies. Planar logarithmic spirals are associated with the simplest such energy, the conformal arc-length, and their remarkable properties follow as a consequence of this invariance and the manner of its breaking. In this paper their three-dimensional analogues will be constructed explicitly. The qualitative behavior of these states is controlled by two parameters, the conserved scaling current  $S$  and the magnitude of the torque  $M$ . The corresponding conservation laws determine the curvature and the torsion. If the spiral apex is located at the origin, the conserved *special* conformal current vanishes. The identities that follow permit the spiral trajectory to be traced in the spherical polar coordinate adapted to the spiral apex and the torque axis. Planar logarithmic spirals sit where  $M$  and  $S$  are tuned such that  $4MS = 1$  in parameter space. More generally, the spiral exhibits internal structure, nutating between two cones aligned along the torque axis. It expands monotonically as this pattern precesses about this axis. If  $4MS < 1$  and  $2S < 1$  the planar spiral undergoes a discontinuous transition into an expanding deformed helical spiral, bounded between two nested similarly oriented cones. If  $4MS > 1$ , however, the cones are identical and oppositely oriented; the torsion changes sign within the nutation cycle where the projection along the torque axis reverses. This transition may be continuous or discontinuous. I will describe the internal structure of the irreducible nutating segment of a spiral and how it gets replicated to generate the complete self-similar geometry. These elementary spirals provide the natural templates against which to compare spiral patterns exhibiting self-similar behavior. In particular, supercritical trajectories (with  $4MS > 1$ ) approximate rather well the nutating tip of the growing tendril in a climbing plant first described by Darwin. This is probably not a coincidence.

Keywords: Conformal Invariance, Vanishing Tension, Self-Similarity, Spirals

## 1 Introduction

Planar logarithmic spirals are the simplest self-similar curves. They also form the most prominent morphological feature of galaxies and weather patterns, the shells of mollusks and the seed heads of plants. Both the cochlea of the inner ear and the pattern of nerve cells in the cornea also display this unmistakable pattern. It would appear that logarithmic spirals are found in nature on any scale in which one can meaningfully speak of a curve. The process of formation of each of these structures is clearly very different; the self-similarity they share would, however, appear to implicate conformal symmetry—invariance under transformations preserving angles—in the process, or emergent within it. This point was grasped in the context of biological growth by D'Arcy Thompson over a hundred years ago in his groundbreaking treatise *On Growth and Form* [1]. We will argue that self-similar patterns are the tension-free states of conformally invariant energies, the vanishing tension breaking this symmetry.

If the overall morphology is not self-similar; the effective geometrical degrees of freedom describing the self-similar spiral must somehow decouple from the larger system to produce this pattern. Self-similar spirals also need not be planar: any of the examples mentioned are, at best, planar only in approximation. To cite two recent studies: the *warped* spiral geometry of our own Milky Way has been attributed to torques generated within the inner disk [2]. What form the three-dimensional spiral geometry assumes is an issue of another order. It has also been argued that the spiral geometry of the Cochlea does not appear to fit a logarithmic template, overturning previous assumptions [3]. This *failure* to fit the template, in itself, is not too surprising: the constraint imposed by its confinement within the skull

most certainly will introduce a length scale inconsistent with self-similarity, so as to frustrate access to the logarithmic form. In this context, the limits on the validity of conformal invariance in biological growth due to constraints have been discussed persuasively, with admirable understatement, by Milnor [4]. The cochlea is not a planar structure. Even if it does display self-similarity, the projections of a self-similar spiral are not generally logarithmic so conclusions arrived at by comparing its projection to planar logarithmic templates should be weighed accordingly. The constraints on the cochlear geometry most likely do account for the observed deviations from a self-similar form; but deviations of the projected spiral from a logarithmic template, as we will explain, are not unexpected. D'Arcy Thompson dedicated a whole chapter to three dimensional self-similar spiral geometries which makes for fascinating reading. It is remarkable that he did this without the benefit of a handle on the mathematics to describe these geometries. Stranger still, in view of the enormous influence of his work, there has not been a systematic attempt to characterize the spatial analogs of logarithmic spirals, never mind building on his taxonomy. In a companion paper [5], a framework was developed to understand how self-similar curves arise due to symmetry breaking in a conformally invariant mechanical system. Here the framework developed in [5] is used to construct the three-dimensional self-similar analogues of the logarithmic spiral. The conical helices familiar in the computer graphics literature (eg. [6]) turn out to be among them but they are far from generic; neither are they the most interesting. Whereas logarithmic spirals are characterized by a single parameter (the angle that the tangent makes with the radial direction from the spiral apex), their three-dimensional counterparts are characterized by two. This extra parameter characterizes an internal structure without any planar analog. Teasing out this structure is the task here.

Conformal invariance also plays an essential role in the study of membranes. The symmetric bending or Willmore energy of a two-dimensional surface is a conformal invariant [7], its analog along curves, the Euler Elastic bending energy, quadratic in the Frenet curvature, is not even scale invariant never mind conformally invariant. It may, at first, seem discouraging that there are no local conformal invariants one can construct without introducing higher derivatives as well as rational powers. The conformal arc-length, given by [8, 9],

$$H = \int ds (\kappa'^2 + \kappa^2 \tau^2)^{1/4}, \quad (1)$$

is not just the simplest, it is also unique at this order. Here  $\kappa$  and  $\tau$  are the Frenet curvature and torsion,  $s$  is arc-length and prime denotes a derivative with respect to  $s$ .  $H$  is also, up to an overall factor, the unique conformal invariant involving these variables and their first derivatives.

Logarithmic spirals are planar critical points of  $H$  [10, 11]. They are also tension-free. Otherwise, they would possess a length scale, inconsistent with self-similarity. The counterparts of logarithmic spirals in three dimensions are the tension-free critical points of (1).

In [5], the conserved currents associated with conformal invariance, the tension  $\mathbf{F}$ , the torque  $\mathbf{M}$ , the scaling current  $S$  and the special conformal current  $\mathbf{G}$  were identified. Here we will examine explicitly how the vanishing of the tension propagates through the remaining conservation laws.

The two independent parameters characterizing tension-free curves are the magnitude of the torque  $M$  and the scaling current  $S$ . This independence contrasts sharply with the planar problem where the two are constrained to follow  $4MS = 1$  [11].

Setting the tangential tension to zero, the conserved scaling current  $S$  constrains the Frenet torsion in terms of the curvature. It also bounds its magnitude, while places a lower bound on the monotonic falloff of the Frenet curvature along the spiral.

Modulo the vanishing tension, the conservation of torque provides a quadrature for the dimensionless variable  $\kappa'/\kappa^2$  with a potential controlled by the parameters  $M$  and  $S$ . This determines  $\kappa$  (and  $\tau$ ) as a function of arc-length; so in principle, one could stop here and use the fundamental theorem of curves to reconstruct the trajectory in space [12]. If one's primary interest were to render trajectories, it would not be remiss to stop here; but we would be at a loss to understand the strikingly consistent self-similar structure they reveal. This is provided by the special conformal current, and as explicitly as one could have hoped for. In a tension-free state, this current may not be translationally invariant in equilibrium, but it transforms by a constant vector. If the origin is located at the spiral apex, the current vanishes. Modulo the torque quadrature, this vector identity reveals internal structure of the spiral geometry that is

not evident in its Frenet data: irreducible cycles are identified describing how the spiral nutates between two fixed circular cones, their common apex coinciding with the spiral apex, their common axis aligned (or anti-aligned) with the torque direction. The precession of this pattern about the torque axis proceeds without switchbacks; the spiral grows monotonically out from its apex. Scaled and rotated accordingly, the complete spiral is generated by iterating a single cycle.

In parameter space Bernoulli's planar logarithmic spirals sit where  $M$  and  $S$  are fine-tuned to their planar values:  $4MS = 1$ . Both subcritical ( $4MS < 1$ ) and supercritical ( $4MS > 1$ ) spirals exist. They are also qualitatively very different.

If  $4MS > 1$ , the spiral nutates between two identical oppositely oriented cones as it expands, the torsion changing sign within each nutation cycle, the precession of these cycles forming an expanding *rosette* bounded by the two cones. The sign change is correlated with the reversal of the projection along the torque axis. Just as a growing planar logarithmic spiral intersects all lines on the plane, these *supercritical* spirals will intersect every plane as they grow. As such, they may be thought of as the genuine three-dimensional analogs of the logarithmic spiral.

Not all supercritical spirals correspond to continuous deformation of a planar logarithmic spiral. This requires a lower bound on  $S$ : if  $2S > 1$ , the conical opening tends smoothly towards  $\pi/2$  as  $4MS \downarrow 1$ , coinciding with a planar logarithmic spiral; if  $2S < 1$ , however, the polar angle defining the conical opening tends in this limit towards an angle, strictly less than  $\pi/2$ , so that the limiting spiral is neither planar nor logarithmic, nor does it oscillate. Yet, if  $M$  is large, the distinction between large and small  $S$  dissolves: the limiting cones close onto the poles so that the spiral nutates from one pole to the other, free to range throughout three-dimensional space.

The naive analogues of logarithmic spirals—expanding helices on a cone—do occur but they never occur as small deformations of logarithmic spirals. In general, spirals with  $4MS < 1$  nutate between two coaxial cones oriented alike, as they rise monotonically along the torque axis. As  $4MS \uparrow 1$ , the outer cone opens into a plane but its inner counterpart does not; the asymptotic behavior of the limiting spiral is logarithmic; its behavior near its apex is not. We will show that, as different as the approach to the limit may be from above and below, the two limiting geometries  $4MS \rightarrow 1$  coincide.

Subcritical spirals provide templates for the growing chambers of a mollusk, If  $2S > 1$ , and  $M$  is not too large, supercritical spirals would appear to track the out-of-plane trajectories of the arms of spiral galaxies. Supercritical spirals could also be providing a clue to better understanding an intriguing process in plant biology: the spiraling motion of the tip of the growing tendril of a cucumber or any other climbing plant, described by Charles Darwin, and dubbed circumnutation by him [13]. A relatively recent review from a plant biologist's perspective is provided in reference [14]. It is also quite instructive to look at one of the numerous time lapse videos posted on youtube illustrating the very elaborate exploration of its spatial environment made by the tendril as it grows [15]. The trajectory of its tip approximates at least qualitatively over several revolutions one of the tension-free supercritical trajectories described here. It can be argued that this is probably no accident: gravity may select the torque axis, but in a first approximation, the tendril does not have an external yardstick against which to assess its progress through its environment. In a single cycle, one would be forgiven for mistaking the trajectory for a simple conical corkscrew, typically adopted by growing seedlings; tendril growth, however, serves a very different purpose: searching for and finding a branch it can attach to; if it fails the tendril will wither and die. Evolutionary pressure is likely to have selected an optimal search strategy to find this support without the benefit of a marker to assess its progress. The projected *rosette* patterns, described and illustrated qualitatively in [14], can be approximated by a supercritical spiral with a large  $4MS$  ratio. In this regime, the growth rate is the lowest. If this conjecture is correct, one would expect conformal invariance to occur as an emergent symmetry, albeit approximate, of the equations determining the progress of the tip. One should not, of course, conflate the dynamical trajectory (the motion of the tendril tip) with the conformation of the tendril itself. First, of course, it would be useful to put the conjecture to the test: tracing the tendril trajectories and comparing them to self-similar templates. Curiously, the first systematic effort to trace these trajectories in a quantitative way is quite recent [16]; the focus, however, has been on the upward motion of seedlings. Unlike tendril growth, there is no reason to expect the trajectory to be self-similar. A challenge for the future is to construct a model predicting the tendril trajectory. In this context, it is noteworthy that a recent mathematical model of the motion of growing seedlings does predict conical helices [17].

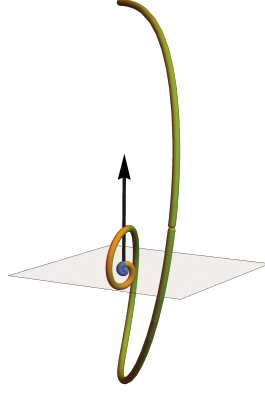


Figure 1: Three consecutive cycles (blue, yellow, green) of a supercritical self-similar spiral with large  $M$  and closing cones. The corresponding logarithmic spiral is orthogonal to the torque direction  $\mathbf{M}$ . Its progress through three dimensional space is captured by the projection of the trajectory onto a unit sphere, illustrated in Figure 20.

Supercritical spirals also provide a pointer towards a solution of a not-unrelated three-dimensional analog of a two-dimensional problem addressed in the computer science literature [18]. A hapless swimmer is lost at sea and cannot see the shore (a line), nor is it known how far away it is. What course should they navigate to improve their odds of reaching this shore? It has been conjectured that it must be a logarithmic spiral. It was also noted in [18] that *The three-dimensional analog, for which shores are planes in space, would seem to be very difficult. We wonder if an appropriate extension of spiral has ever been examined in the past.* It appears that natural selection has been nudging the growing plant tendril towards a solution of this scale-free three-dimensional problem for the past 200 or so million years.

## 2 The Conserved Currents

We consider then an arc-length parametrized curve  $s \rightarrow \mathbf{X}(s)$  in three-dimensional Euclidean space with the inner product between two vectors denoted by a centerdot separating them.

Let prime denote a derivative with respect to arc-length so that  $\mathbf{t} = \mathbf{X}'$  is the unit tangent vector to the curve. Also let  $\{\mathbf{t}, \mathbf{N}, \mathbf{B}\}$  denote the Frenet frame adapted to this curve. The acceleration is directed along  $\mathbf{N}$ , so that  $\mathbf{t}' = -\kappa \mathbf{N}$ , where  $\kappa$  is the Frenet curvature;  $\mathbf{N}' = \kappa \mathbf{t} - \tau \mathbf{B}$ , and  $\mathbf{B}' = \tau \mathbf{N}$ .

In [5], the Euler Lagrange equations and conserved currents associated with the conformally invariant energy (1) were derived. The most general conformal transformation induced on the curve is of the form,

$$\delta \mathbf{X} = \mathbf{a} + \mathbf{b} \times \mathbf{X} + \lambda \mathbf{X} + \delta_c \mathbf{X}, \quad (2)$$

consisting of a translation  $\mathbf{a}$ , a rotation characterized by its axial vector  $\mathbf{b}$ , rescaling by  $\lambda$  and a special conformal transformation  $\delta_c \mathbf{X}$  (the composition of an inversion in a sphere with a translation followed by a second inversion, linearized in the intermediate translation  $\mathbf{c}$ ), given by  $\delta_c \mathbf{X} = |\mathbf{x}|^2 \mathbf{R}_\mathbf{X} \mathbf{c}$ , where  $\mathbf{R}_\mathbf{X}$  is the linear operator describing a reflection in the plane orthogonal to  $\mathbf{X}$ ,  $\mathbf{R}_\mathbf{X} = 1 - 2\hat{\mathbf{X}} \otimes \hat{\mathbf{X}}$ . If the energy is conformally invariant,

$$\int ds \mathbf{F}' \cdot \delta \mathbf{X} + \int ds \mathcal{J}' = 0, \quad (3)$$

where

$$\mathcal{J} = \mathbf{a} \cdot \mathbf{F} + \mathbf{b} \cdot \mathbf{M} + \lambda S + \mathbf{c} \cdot \mathbf{G}. \quad (4)$$

Here  $\mathbf{F}$  is the tension,  $\mathbf{M}$  is the torque,  $S$  and  $\mathbf{G}$  are the scaling and special conformal currents respectively. In equilibrium,  $\mathbf{F}' = 0$  and each of the currents is conserved:  $\mathbf{F}$ ,  $\mathbf{M}$ ,  $S$ , and  $\mathbf{G}$  are constant.

When  $H$  is the conformal arc-length (1), the torque is given by [5]

$$\mathbf{M} = \mathbf{X} \times \mathbf{F} - H_1 \mathbf{N} + H_2 \mathbf{B} - 2\mathcal{S}_{12} \mathbf{t}, \quad (5)$$

where

$$2H_1 = -(\mu^3 \kappa')' + \mu^3 \kappa \tau^2; \quad (6a)$$

$$2H_2 = -(\mu^3 \kappa^2 \tau)' / \kappa; \quad (6b)$$

$$2\mathcal{S}_{12} = -\mu^3 \kappa^2 \tau / 2, \quad (6c)$$

and the shorthand

$$\mu = (\kappa'^2 + \kappa^2 \tau^2)^{-1/4} \quad (7)$$

is introduced. The scaling current is given by

$$S = -\mathbf{F} \cdot \mathbf{X} + S_D, \quad (8)$$

where

$$S_D := -\partial \mathcal{H} / \partial \kappa' \kappa = -\mu^3 \kappa \kappa' / 2. \quad (9)$$

Finally the special conformal current is given by

$$\mathbf{G} = 2\mathbf{X} \times (\mathbf{M} - \mathbf{X} \times \mathbf{F}) - |\mathbf{X}|^2 \mathbf{F} - 2S \mathbf{X} - \mu^3 (\kappa' \mathbf{N} + \kappa \tau \mathbf{B}), \quad (10)$$

involving the three conserved currents  $\mathbf{F}$ ,  $\mathbf{M}$  and  $S$ .

Notice that  $S$  and  $\mathbf{M}$  possess the same dimensions as the energy,  $H$ . As such they are dimensionless. The tension has dimensions of inverse length, and conformal current  $\mathbf{G}$  has the dimension of length. The attentive reader will notice that an explicit expression for  $\mathbf{F}$  has not been written down: this is because it is never used explicitly in this paper. It is constructed explicitly in reference [5].

### 3 Tension-free States

Our proposition in this paper is to construct the tension-free stationary states of  $H$  and to show that these states are self-similar.

#### 3.1 Conserved scaling current in tension-free states

If  $\mathbf{F} = 0$ , Eq.(8) implies that  $S_D$  itself will be conserved. Using the identity Eq.(9), the conservation law can be cast as the statement

$$\mu^3 \kappa \kappa' / 2 = -S, \quad (11)$$

where  $S$  is the constant value of the scaling current ( $\kappa' < 0$ ). Introducing the dimensionless ratios  $\Sigma$  and  $\Gamma$ , defined by

$$\Sigma = (-) \frac{\kappa'}{\kappa^2}; \quad \Gamma = \frac{\tau}{\kappa}, \quad (12)$$

Eq.(11) can be recast as an algebraic constraint on these two variables:

$$[\Sigma^2 + \Gamma^2]^3 = \frac{1}{16S^4} \Sigma^4; \quad (13)$$

equivalently

$$\Gamma^2 = \Sigma^2 \left( \frac{1}{(4S^2 \Sigma)^{2/3}} - 1 \right). \quad (14)$$

The torsion is completely determined by the curvature. To avoid the fractional powers appearing in Eq.(14), introduce a change of curvature variable and parameter,  $\gamma$ :

$$Z = \Sigma^{2/3} > 0; \quad (15a)$$

$$\gamma = (2S)^{-4/3}. \quad (15b)$$

With respect to these variables Eq.(14) assumes the simple quadratic form

$$\Gamma^2 = Z^2(\gamma - Z). \quad (16)$$

Let us now examine the consequences of this constraint.

### 3.1.1 Vanishing torsion and a lower bound on $\kappa$

It is immediately clear that the torsion vanishes when either  $Z = 0$  or  $Z = \gamma$ . As will be clear in section 3.3,  $Z = 0$  is inaccessible. The torsion can thus only change sign if  $Z = \gamma$ . The conservation of torque will also determine under what conditions this value of  $Z$  is accessible.

Eq.(16) places an upper bound on  $Z$ :  $Z \leq \gamma$ , which is saturated when  $\tau = 0$ . In terms of  $\Sigma$ ,

$$|\Sigma| \leq \frac{1}{(2S)^2}; \quad (17)$$

if  $Z = \gamma$  or  $\Sigma = 1/(2S)^2$  everywhere, the curve will be planar with  $\kappa = (2S)^2/s$ , which describes a logarithmic spiral. Details can be found in reference [11] as well as in Appendix A.

Suppose that  $\kappa'$  is negative somewhere. We will see in the next subsection that  $Z$  or  $\Sigma$  never vanishes; this implies that  $\kappa'$  is negative everywhere. Thus the curvature decreases monotonically with  $s$ . Integrating across the inequality (17) then implies that

$$\kappa s \geq 4S^2. \quad (18)$$

Thus the scaling current  $S$  places a lower bound on the falloff of  $\kappa$ . This justifies the interpretation of  $S$  as a dimensionless measure of curvature.

### 3.1.2 An upper bound on $\tau$

It is evident from Eq.(16) that  $\Gamma$  has a maximum, which occurs when  $Z_{\tau \max} = 2\gamma/3$  if this value of  $Z$  is accessible. We thus possess the bound on  $\tau$  by  $\kappa$

$$\tau^2 \leq 4\gamma^3 \kappa^2 / 27 = \kappa^2 / (108S^4). \quad (19)$$

Thus scale invariance bounds the magnitude of the torsion by the curvature. Significantly, the bounds (18) and (19) are independent of the magnitude of the torque  $M$ .

Eq.(13) suggests the existence of non-planar equilibrium states with constant values of both  $\Sigma$  and  $\Gamma$  which would correspond, as described in Appendix A, to logarithmic helices. The conservation of torque will, however, imply that  $Z$  is not constant unless the magnitude of the torque is fine-tuned, and  $S$  itself is bounded:  $2S < 1$ .

## 3.2 Torque conservation provides a quadrature for $\Sigma$

Let us now explore the consequences of torque conservation in tension-free states.

In a tension-free state, the constant torque vector defined by Eq.(5), like  $S$ , becomes translationally invariant; it will define the spiral axis. Its squared magnitude,  $\mathbf{M}^2$ , like  $S$  is Euclidean invariant. We will now show that it provides a quadrature for  $\Sigma$ , modulo the conservation of  $S$  as captured by Eq.(14)) which allows  $\Gamma = \tau/\kappa$  to be eliminated in favor of  $\Sigma$ .

To see this, note that, along tension-free curves, the expressions for  $H_1$ ,  $H_2$  and  $S_{12}$  appearing in Eq.(5), given by Eqs.(6), simplify:

$$\begin{aligned} H_1 &= S[(1/\kappa)' - \tau^2/\kappa'] = -S[(\kappa'/\kappa^2)^2 + (\tau/\kappa)^2](\kappa^2/\kappa') \\ &= S[\Sigma^2 + \Gamma^2]/\Sigma = S\gamma Z^{1/2}; \end{aligned} \quad (20a)$$

$$\begin{aligned} H_2 &= S(\kappa\tau/\kappa')'/\kappa = -S[\Gamma/\Sigma]'/\kappa = -S[\Gamma/\Sigma]^\bullet \\ &= \text{sign}(\tau)S\gamma Z^\bullet/(2Z^{3/2}(\gamma - Z)^{1/2}); \end{aligned} \quad (20b)$$

$$2S_{12} = S\kappa\tau/\kappa' = S\Gamma/\Sigma = \text{sign}(\tau)S(\gamma - Z)^{1/2}/Z^{1/2}, \quad (20c)$$

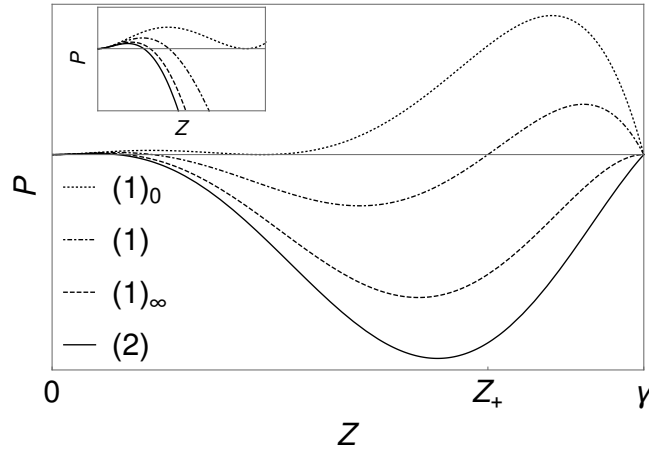


Figure 2: The potential for fixed  $\gamma = 2$ .  $(1)_0$   $m = 2.16$  (the two roots of the quadratic coincide within the interval  $[0, 2]$ );  $(1)$   $m = 2.5$  (the two roots lie within the interval  $[0, 2]$ );  $(1)_\infty$   $m = 2.828$  (the larger root occurs at  $Z = 2$ );  $(2)$   $m = 3$  (the larger root lies outside the interval).  $Z_+$  is indicated in case (1); in general it moves from left to right as  $m$  increases. The qualitative behavior of the state will depend sensitively on the value of  $m$  as described in section 3.3

where, for the expressions involving  $Z$  and  $Z^\bullet$ , the identities

$$(\Gamma/\Sigma)^2 = \gamma Z^{-1} - 1; \quad (21a)$$

$$(\Gamma/\Sigma)^\bullet = -\text{sign}(\tau)\gamma Z^\bullet / (2Z^{3/2}(\gamma - Z)^{1/2}), \quad (21b)$$

following from Eq.(14) and the definitions following it, have been used. In Eq.(20b) and (21b) we have also introduced the variable  $\Theta$ , defined by  $d\Theta = \kappa ds$ ; the dot (or bullet) from here on signifies a derivative with respect to  $\Theta$  (not conformal arc-length as used in reference [5]).

Using Eq.(5) with  $\mathbf{F} = 0$ , the constant magnitude of the torque  $M^2 = \mathbf{M}^2$  is now given by

$$\begin{aligned} \mathbf{M}^2 &= H_1^2 + H_2^2 + 4S_{12}^2 \\ &= S^2 \left( \gamma^2 Z + \gamma^2 \frac{Z^{\bullet 2}}{4Z^3(\gamma - Z)} + \gamma/Z - 1 \right), \end{aligned} \quad (22)$$

where the identities collected in Eqs.(20) have been used on the second line. The distinction between positive and negative torsion does not play a role yet. Eq.(22) can be rearranged to provide the quadrature for  $Z$ :

$$\frac{\gamma^2}{4} Z^{\bullet 2} + P(Z; \gamma, m) = 0, \quad (23)$$

where the potential  $P$  is the fifth order polynomial given by

$$P = Z^2(\gamma - Z) \left[ \gamma^2 Z^2 - (m^2 + 1)Z + \gamma \right]. \quad (24)$$

We have introduced the normalized torque  $m$ , defined by

$$m^2 = M^2 / S^2. \quad (25)$$

The quadrature Eq.(23), unlike Eq.(16) (or, equivalently, Eq.(14)), involves both the torque  $M$  and the scaling current  $S$  through  $m$  and  $\gamma$ . Each admissible set of values of  $\gamma$  and  $m$  will parametrize a unique tension-free state. The potential is plotted with a fixed value  $\gamma = 2$ , for various significant values of  $m$  in Figure 2.

### 3.3 Motion of a particle in a potential

The quadrature can be interpreted in terms of the motion of a particle in a potential. For the moment one can ignore the fact that  $Z$  (or indeed  $\Sigma$ ) is a composite variable, involving derivatives of the Frenet curvature.

The potential  $P$  possesses a double root at  $Z = 0$  and another at  $Z = \gamma$ .  $Z$ , by definition, is positive and Eq.(17) constrains  $Z \leq \gamma$ . The two roots of the quadratic are given by

$$Z_{\pm} = \frac{(m^2 + 1)}{2\gamma^2} \pm \frac{1}{2\gamma^2} \sqrt{(m^2 + 1)^2 - 4\gamma^3}. \quad (26)$$

If these roots are not real, the potential will be positive everywhere within the interval  $[0, \gamma]$  and, as a consequence the only accessible values of  $Z$  are  $Z = 0$  and  $Z = \gamma$ , corresponding respectively to a circle and a planar logarithmic spiral.

**The origin  $Z = 0$  is isolated:** We note that the smaller root  $Z_-$  is strictly positive for all finite  $m$ ; this implies that the origin remains isolated: as a consequence there are no tension-free deformations of a circle. Whereas Eq.(16) did not rule out  $\tau$  vanishing at  $Z = 0$ , the quadrature does:  $\tau = 0$  if and only if  $Z = \gamma$ .

**A lower bound on the torque:** The reality of the roots in 26) places a lower bound on  $m$ :

$$(m^2 + 1)^2 \geq 4\gamma^3. \quad (27)$$

Eq.(28) defines a curve in parameter space, indicated  $\mathcal{C}_0$  in Figure 3. Parameter values below this curve do not describe tension-free states. It presents a lower bound on the torque.

**Saturating the lower bound on the torque:** If  $m$  and  $\gamma$  are tuned such that

$$(m^2 + 1)^2 = 4\gamma^3, \quad (28)$$

the two roots of the quadratic coincide,  $Z_+ = Z_0 = Z_-$ , with  $Z_0 = (m^2 + 1)/2\gamma^2 = \gamma^{-1/2}$ , or equivalently,  $\Sigma_0 = 2S$ .

**Conical Helices (1)<sub>0</sub>:**  $(m^2 + 1)^2 = 4\gamma^3$ ,  $\gamma \geq 1$

To be accessible, the coincident root must also lie below  $Z = \gamma$ , the bound derived in section 3.1.1. This requires  $\gamma \geq 1$  (or equivalently  $2S \leq 1$ ). A representative potential is traced in Figure 2 for  $\gamma = 2$ , where it is labeled (1)<sub>0</sub>.

These states will be constructed explicitly in Appendix B. They correspond to rising spirals helices wound upon a circular cone. While these trajectories correspond to one's intuitive guess of the three dimensional self-similar analogue of a logarithmic spiral, they are in no sense generic, requiring fine both the fine-tuning of  $m$  and  $\gamma$ , as well as a lower bound on  $\gamma$ .

**Deepening the well:** When Eq.(27) is satisfied with strict inequality, the quadratic possesses two distinct positive roots. Three possibilities can be distinguished which depend on the location of  $Z_-$  and  $Z_+$  with respect to  $Z = \gamma$ : both  $Z_-, Z_+ < \gamma$ ;  $Z_- < \gamma < Z_+$  and both  $Z_+, Z_- > \gamma$ . One of these two roots must also lie below  $\gamma$  for otherwise the potential is not accessible. This rules out the third possibility just as it did with coincident roots. The condition  $Z_+ = \gamma$  separating the remaining two options is given by

$$m^2 = \gamma^3, \quad (29)$$

represented by curve  $\mathcal{C}_1$  in parameter space (see Figure 3). The boundary curves  $\mathcal{C}_0$  and  $\mathcal{C}_1$  touch with a common tangent at the point (1, 1) on the  $(\gamma, m)$  plane.

**Subcritical Torque (1) :**  $2\gamma^{3/2} - 1 < m^2 < \gamma^3$   $\gamma \geq 1$

Within the region of parameter space bounded between  $\mathcal{C}_0$  and  $\mathcal{C}_1$ ,  $Z_+$  is bounded from above and  $Z_-$  from below:  $Z_+ < [\gamma^3 + 1 + |\gamma^3 - 1|]/2\gamma^2$ ,  $Z_- > [\gamma^3 + 1 - |\gamma^3 - 1|]/2\gamma^2$ .

If  $\gamma > 1$ , then  $Z_+ < \gamma$ . In Figure 2, the potential, labeled (1) is traced for parameter values  $\gamma = 2$ ,  $m = 2.5$ .  $Z$  oscillates within the band  $[Z_-, Z_+]$ , which does not include the point  $Z = \gamma$ . As such, the torsion never vanishes. Such states correspond to deformed helices bounded, as explained in section 5, between two cones. The two cones



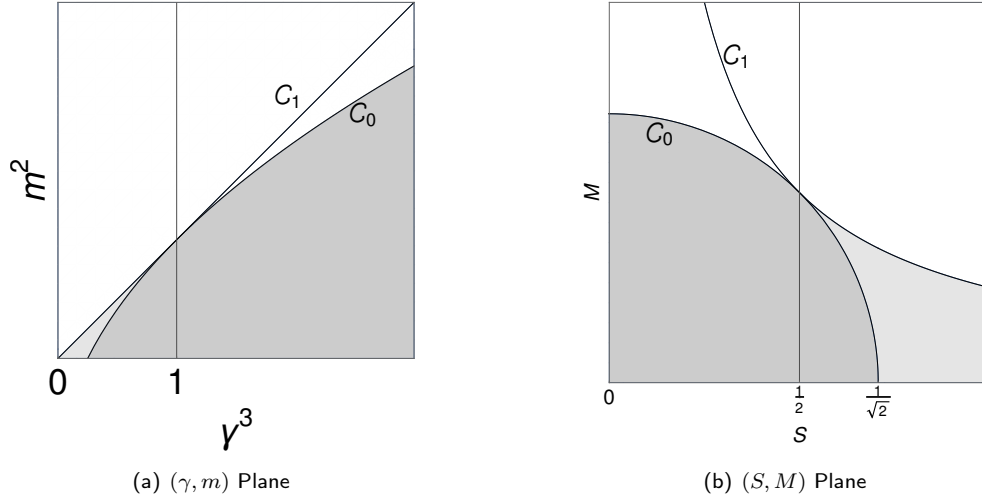


Figure 3: Parameter Space: The curves  $\mathcal{C}_0$  and  $\mathcal{C}_1$ , defined respectively by  $(m^2 + 1)^2 - 4\gamma^3 = 0$  and  $m^2 = \gamma^3$ , are displayed in Figure 3 (a). Their representation with respect to the original parameters  $M$  and  $S$  are displayed in (b):  $\mathcal{C}_0$  is defined by  $M^2 + S^2 = 1/2$ ;  $\mathcal{C}_1$  is defined by  $4MS = 1$ .  $\mathcal{C}_0$  and  $\mathcal{C}_1$  touch with a common tangent at a single point  $\gamma = 1 = m$ , or equivalently  $S = 1/2 = M$ . (i) Logarithmic spirals sit on the phase boundary  $\mathcal{C}_1$ . Approached from above and below  $\mathcal{C}_1$  also represents limiting supercritical and subcritical spirals. If  $\gamma < 1$  the supercritical limit is continuous; if  $\gamma > 1$  the two limits coincide and is not a logarithmic spiral. (ii) The (gray) region below  $\mathcal{C}_0$ , as well as the (light gray) region bounded between  $\mathcal{C}_0$  and  $\mathcal{C}_1$  when  $\gamma < 1$  ( $S > 1/2$ ), are not accessed in tension-free states. This breaks the (unexpected) symmetry between  $M$  and  $S$  in Figure 3 (b). (iii) Each point along  $\mathcal{C}_0$  with  $\gamma > 1$  represents a conical helix. (iv) Between  $\mathcal{C}_0$  and  $\mathcal{C}_1$  and  $\gamma > 1$ , the spiral nutates between two coaxial cones with the same orientation (See section 4); (v) Above  $\mathcal{C}_1$ , the spiral nutates between identical coaxial cones with opposite orientations. (vi)  $\mathcal{C}_0$  and  $\mathcal{C}_1$  coincide when  $\gamma = 1 = m$  or  $S = 1/2 = M$ . Additional structure, not evident in the quadrature, will become apparent as the consequences of the conserved special conformal current are processed.

coalesce when the roots coincide:  $Z_- = Z_+$ .

If, on the other hand,  $\gamma < 1$ , then  $Z_- > 1 > \gamma$ , so that the well is inaccessible. Thus the region of parameter space below  $\mathcal{C}_1$  is inaccessible when  $\gamma < 1$ . This forbidden region is indicated in light gray in Figure 3.

### Supercritical Torque (2): $m^2 > \gamma^3$

Now  $Z_+ > \gamma$  for all  $\gamma$ , and  $Z_- < \gamma$ . The upper turning point in the potential well occurs always at  $Z = \gamma$  and  $Z$  oscillates within the band  $[Z_-, \gamma]$ . Such a potential, labeled (2), is traced in Figure 2 for the parameter values,  $\gamma = 2$ ,  $m = 3$ . According to Eq.(16), the torsion  $\tau$  vanishes at the upper turning point  $Z = \gamma$ , changing sign upon turning. When the special conformal current is examined in section 4, it will be seen that the sign of  $\tau$  correlates directly with the rise and fall of the spiral along the torque axis.

Now examine more closely what occurs in the neighborhood of  $\mathcal{C}_1$ .

### Logarithmic Spirals (2)<sub>0</sub>: $m^2 = \gamma^3$

If  $m$  and  $\gamma$  are fine-tuned to lie along  $\mathcal{C}_1$ , there is an equilibrium perched at  $Z = \gamma$  with  $\tau = 0$ . These are planar logarithmic spirals.

The behavior in the neighborhood of the boundary  $\mathcal{C}_1$  in parameter space depends sensitively on whether  $\gamma < 1$  or  $\gamma > 1$ .

### Asymptotically Logarithmic Helical Spirals (1)<sub>∞</sub>: $m^2 \uparrow \gamma^3$ ; $\gamma > 1$

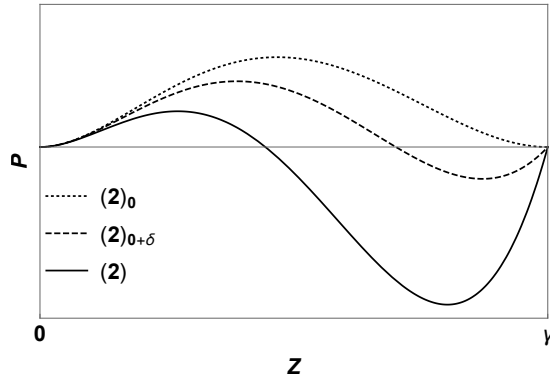


Figure 4: The potential for fixed  $\gamma = .75$ , and  $m = 0.75^{3/2}, 0.85^{3/2}$  and  $1.3^{3/2}$ . Continuous supercritical deformations of logarithmic spirals require  $\gamma < 1$ .

As  $m^2 \uparrow \gamma^3$ , in the subcritical region,  $Z_+ \uparrow \gamma$ , whereas  $Z_- = 1/\gamma^2 \ll \gamma$  unless  $\gamma \approx 1$ . On this approach, both  $\kappa$  and  $\tau$  (with a fixed sign) undergo large deformations about the helical value with a growing period of oscillation. Asymptotically,  $Z_+$  sits on  $Z = \gamma$  which is now a double root of the potential, with negative curvature, indicated  $(1)_\infty$  in Figure 2. In this limit, the period of oscillation  $\Theta_0 \rightarrow \infty$ . With it,  $\tau \rightarrow 0$  and  $\kappa \rightarrow 2S/s$ , so that the spiral fans out asymptotically into a planar logarithmic spiral. The large non-planar deviations persist towards the center. The important upshot is that there are no small subcritical deformations of logarithmic spirals.

#### Asymptotically Logarithmic Helical Spirals $(2)_\infty$ : $m^2 \downarrow \gamma^3$ with $\gamma > 1$

The limiting well is large and identical to  $(1)_\infty$  in Figure 2. Because  $Z_+ > \gamma$  in the approach to the limit, both  $\kappa$  and  $\tau$  undergo large oscillations about the logarithmic value (the sign of  $\tau$  alternates) but, in the limit, the period of oscillation diverges so that  $\tau$  no longer gets to change sign. Though the approaches to the limit are very different, the limiting trajectories  $(1)_\infty$  and  $(2)_\infty$  are identical. There are no continuous supercritical deformations of a logarithmic spiral if  $\gamma > 1$ .

#### Deformations of Logarithmic Spirals $(2)_0$ : $m^2 \downarrow \gamma^3$ , $\gamma < 1$

Let  $\gamma < 1$ . The limiting behavior as  $m^2 \downarrow \gamma^3$ , as well as its approach, are displayed in Figure 3.3 for  $\gamma = .75$ . If  $\delta m^2 = m^2 - \gamma^3$  is small and positive, it is simple to show that the well is small. Use Eq.(26) to approximate the lower turning point:  $Z_- \approx \gamma - 2\gamma\delta m^2/(1 - \gamma^3)$ , whenever  $\delta m^2/\gamma^3 \ll 1$ . Thus the well between  $Z_-$  and  $\gamma$  is both narrow and shallow and the motion within it describes small oscillations about a logarithmic spiral. All small deformations of logarithmic spirals are of this form.

### 3.4 Expressing $\kappa$ as a function of $s$

For each value of  $S$  and  $M$ , the quadrature determines  $Z$  as a function of  $\Theta = \int \kappa ds$ , given implicitly by

$$\Theta(Z) = -\frac{1}{2} \int_Z^{\min(\gamma, Z_+)} \frac{dZ}{Z \sqrt{(\gamma - Z)(Z_+ - Z)(Z - Z_-)}}. \quad (30)$$

The right hand side can be expressed in terms of an Elliptic function of the third kind. We choose not to dwell on this exact solution of the quadrature, suggesting—misleadingly in our view—that this exact form is essential for an understanding of the equilibrium geometry.

So long as  $Z_+ \neq \gamma$ , the *motion* in the potential is periodic in  $\Theta$ , with period  $\Theta_0 = 2\Theta(Z_-)$ . This is the relevant period if the spiral is subcritical; if it is supercritical, however, the sign change in  $\tau$  at  $Z = \gamma$  doubles the period to  $2\Theta_0$ .

To determine  $\kappa$  as a function of  $s$ , use  $\Sigma = -\kappa'/\kappa^2 = -\kappa^\bullet/\kappa$  to first express  $\kappa$  as a function of  $\Theta$ ,

$$\kappa(\Theta)/\kappa(0) = e^{-\int_0^\Theta d\Theta_1 Z^{3/2}(\Theta_1)}, \quad (31)$$

where  $\kappa(0)$  is simply the value of  $\kappa$  at the zero of  $\Theta$ . It is now clear that  $\kappa$  decreases exponentially with  $\Theta$ , modulated by the oscillation in the well with period  $\Theta_0$ : over one period

$$\kappa_0 = \kappa(\Theta_0)/\kappa(0) = e^{-\int_0^{\Theta_0} d\Theta_1 Z^{3/2}(\Theta_1)}. \quad (32)$$

Simple bounds can now be placed on  $\kappa_0$ , in terms of the turning points and the period:  $e^{-Z_{\max}^{3/2}\Theta_0} \leq \kappa_0 \leq e^{-Z_{-}^{3/2}\Theta_0}$ , where  $Z_{\max} = \text{Min}(Z_+, \gamma)$ . The behavior of  $\kappa_0$  as a function of  $\gamma$  and  $m$  will be taken up in section 9 in the context of scaling and self-similarity. It will be seen that  $\kappa_0^{-1}$  ranges from 0 to 1, indicating rapid and slow dilation per period respectively.

Arc length  $s$  is related to  $\Theta$  by  $s^\bullet = \kappa^{-1}$ , so that

$$s(\Theta) - s(0) = \kappa_0^{-1} \int_0^\Theta d\Theta_1 e^{\int_0^{\Theta_1} d\Theta_2 \Sigma(\Theta_2)}. \quad (33)$$

Arc-length increases exponentially with  $\Theta$ . The constant  $s(0)$  is the arc-length along the spiral from the apex to the position marking  $\Theta = 0$ .

Inverting Eq.(33) and substituting into (31), provides the functional dependence of  $\kappa$  on  $s$ . Note that

$$\kappa' = \frac{\kappa^\bullet}{s^\bullet} = \Sigma(\Theta) e^{-2\int_0^\Theta d\Theta_1 \Sigma(\Theta_1)}. \quad (34)$$

The dependence of the torsion on  $s$  is now determined using Eq.(14) to be

$$\tau(s) = \kappa(s)\Gamma(\Theta(s)). \quad (35)$$

Notice that whereas  $\kappa$  decreases monotonically,  $\tau$  generally does not.

Having determined both the curvature  $\kappa$  and the torsion  $\tau$ , it is possible to appeal to the fundamental theorem of curves to reconstruct the space curve. We are now in a position to show how much better it is possible to do by enlisting the conserved conformal current.

## 4 Conformal current and spatial trajectories

In tension-free states, it was seen that the scaling current is translationally invariant, given by Eq.(11). The constant conformal current (10), given by

$$\mathbf{G}_0/2 = \mathbf{X} \times \mathbf{M} - S \left[ \mathbf{X} - \left( \frac{1}{\kappa} \right) \mathbf{N} - \left( \frac{\tau}{\kappa'} \right) \mathbf{B} \right], \quad (36)$$

is not. In equilibrium, however, it transforms by a constant vector under translation; as a consequence, with a judicious choice of origin, it is always possible to set  $\mathbf{G}_0 = 0$ . This privileged point, perhaps, not surprisingly, turns out to be the spiral apex.

### 4.1 The projection along the torque axis $X_\parallel$

Eq.(36), together with Eq. (5), with  $\mathbf{F} = 0$  and  $\mathbf{G}_0 = 0$ , together imply the identity for the projection of the position vector along the torque axis:

$$X_\parallel = \mathbf{X} \cdot \hat{\mathbf{M}} = \frac{1}{M\kappa} \left( H_2 - \left( \frac{\kappa\tau}{\kappa'} \right) H_1 \right). \quad (37)$$

Make reuse of Eqs. (20a) and (b) to recast the term in brackets appearing on the right hand side of Eq.(37) in terms of  $Z$  and  $Z^\bullet$ :

$$\begin{aligned} H_2 + \left(\frac{\Gamma}{\Sigma}\right) H_1 &= -S \left[ \left(\frac{\Gamma}{\Sigma}\right)^\bullet - \left(\frac{\Gamma}{\Sigma^2}\right) (\Sigma^2 + \Gamma^2) \right] \\ &= \text{sign}(\tau) \frac{S}{Z^{3/2}(\gamma - Z)^{1/2}} \left( \frac{\gamma}{2} Z^\bullet + \gamma Z^{3/2}(\gamma - Z) \right). \end{aligned} \quad (38)$$

The quadrature (23) is now used to eliminate  $Z^\bullet$ , modulo its sign, in favor of the potential so that:

$$X_{\parallel} = \text{sign}(\tau) \frac{\gamma}{m \kappa Z^{1/2}} W_{\pm}(Z), \quad (39)$$

where the shorthands

$$W_{\pm} = \text{sign}(Z^\bullet) Q + Z^{1/2}(\gamma - Z)^{1/2}, \quad (40)$$

as well as

$$Q(Z) = (Z - Z_-)^{1/2}(Z_+ - Z)^{1/2} \geq 0, \quad (41)$$

are introduced in anticipation of the role they will play in tracing trajectories. In general  $W_+ > 0$ , and  $W_+ \geq W_-$ , with equality at the turning points,  $Z_{\pm}$ . Also  $W_- = -W_+$  at  $Z = \gamma$ ; thus  $W_-$  necessarily vanishes somewhere between  $Z_-$  and  $Z = \gamma$ .

### The turning of $X_{\parallel}$ in supercritical spirals

It is easy to show that the extrema of  $X_{\parallel}$  always occur at  $Z = \gamma$ , thus correlating with the changing sign of  $\tau$ . To see this, begin with the simple identity,

$$X'_{\parallel} = \mathbf{t} \cdot \hat{\mathbf{M}}, \quad (42)$$

connecting the velocity along the torque axis to the cosine of the angle  $\Psi$  that the tangent vector along the curve makes with that direction. Now using the definition (5) of  $\mathbf{M}$  with  $\mathbf{F} = 0$ , as well as the identity (20)(c), it is straightforward to express the right hand side of Eq.(42) as a function of  $Z$ , modulo  $\text{sign}(\tau)$ :  $\mathbf{t} \cdot \hat{\mathbf{M}} = -2S_{12}/M = -S\kappa\tau/(M\kappa') = \Gamma/(m\Sigma) = \text{sign}(\tau)(\gamma - Z)^{1/2}/(mZ^{1/2})$  or

$$X'_{\parallel} = \text{sign}(\tau) \frac{1}{m} \frac{1}{Z^{1/2}} (\gamma - Z)^{1/2}. \quad (43)$$

It is also simple to confirm that the magnitude of  $X'_{\parallel}$  is bounded by 1 for all accessible values of  $\gamma$  and  $m$ .<sup>1</sup> The identity (43) has significant consequences:

#### In supercritical trajectories $X_{\parallel}$ oscillates about $X_{\parallel} = 0$

According to Eq.(43),  $X'_{\parallel}$  vanishes at the upper turning point,  $Z = \gamma$ . Suppose that this is a local maximum, and set  $\Theta = 0$  there. As  $\Theta$  increases  $X_{\parallel}$  can only decrease (with  $\tau < 0$ ), passes through zero as the mid-plane is crossed, reaching a minimum when  $Z$  returns to  $\gamma$  where  $\tau$  changes sign and the motion is reversed. Thus supercritical spirals oscillate along the torque axis with period  $2\Theta_0$  with respect to  $\Theta$ , crossing the mid plane twice in each period.

#### In subcritical trajectories $X_{\parallel}$ increases monotonically with arc-length

Along such trajectories  $\tau$  does not change sign (say  $\tau > 0$ ) and  $Z < \gamma$ , Eq.(43) then implies that  $X'_{\parallel} > 0$  and  $X_{\parallel}$  increases monotonically along the spiral, no matter how deformed it may be, and never cross the mid plane.

This remains true in the limiting, asymptotically logarithmic geometries of type(1) $_{\infty}$ . This limiting growth is examined in Appendix E where the sub-linear power law controlling the approach to a planar logarithmic spiral is identified.

<sup>1</sup>It is possible to integrate Eqs.(61) and (43) to provide expressions for  $\rho$  and  $X_{\parallel}$  as functions of  $s$ . Simpler, however, once  $\kappa$  has been determined, is to use the expressions (45) and (39) for  $\kappa\rho$  and  $\kappa X_{\parallel}$  respectively, using the expression (31) for  $\kappa$ .

## 4.2 The polar radius with respect to the spiral apex

With  $\mathbf{G}_0 = 0$ , Eq.(36) implies

$$M^2 X_\perp^2 + S^2 \rho^2 = \frac{S^2}{\kappa^2 \kappa'^2} (\kappa'^2 + \kappa^2 \tau^2) = \frac{S^2 \gamma}{\kappa^2 Z}, \quad (44)$$

where  $\rho = |\mathbf{X}|$  is the polar radius, and  $X_\perp = |\mathbf{X} \times \hat{\mathbf{M}}|$  is the distance to the torque axis. Eliminating  $X_\perp$  in Eq.(44) in favor of  $\rho$  and  $X_\parallel$ , and using Eq.(39) for  $\kappa X_\parallel$ , the identity

$$(m^2 + 1) \kappa^2 \rho^2 = \frac{\gamma}{Z} [\gamma W_\pm(Z)^2 + 1] \quad (45)$$

follows. There is no explicit dependence on torsion. The value of  $\kappa \rho$  depends only on  $Z$  and  $\text{sign}(Z^\bullet)$ .

In section 6, it will be shown that  $\rho' \leq 1$ , and that it is a monotonically increasing function of  $s$ .

If one instead eliminates  $X_\parallel$  in Eq.(44), the identity

$$m^2 X_\perp^2 = \frac{\gamma}{\kappa^2 Z} - \rho^2 \quad (46)$$

follows. Positivity of the left hand side places an upper bound on  $\kappa \rho$  in terms of  $Z$ . The dimensionless variables  $\kappa \rho$  and  $\kappa X_\perp$ , unlike  $X_\parallel$ , are independent of  $\text{sign}(\tau)$ .

## 4.3 The spherical polar angle adapted to M

Using Eqs.(39) and (45), the polar angle that the position vector makes with the torque axis,  $\cos \theta = X_\parallel / \rho$ , can be expressed in the form

$$\cos \theta_{(\pm, \pm)} = \text{sign}(\tau) \frac{\sqrt{m^2 + 1}}{m} \frac{W_\pm(Z)}{\sqrt{W_\pm(Z)^2 + \gamma^{-1}}}. \quad (47)$$

Notice that the explicit dependence on  $\kappa$  in the expressions for  $X_\parallel$  and  $\rho$  cancel. The polar angle depends only on the position within the well.

## 5 Cosine Cycles

The internal structure of a supercritical spiral is captured by the cycle formed by the four functions of  $Z$ , one for each sign pairing  $(-, -)$ ,  $(-, +)$ ,  $(+, -)$  and  $(+, +)$  in Eq.(47). This cycle forms a closed figure of eight in  $(Z, \cos \theta)$  space, as illustrated by the cycle for  $\gamma = 1.2$  and  $m = \sqrt{2}$  displayed in Figure 5 (a). The cycle is completed in two complete oscillations within the potential well, one for each sign of  $\tau$ . Using the functional form  $Z(\Theta)$  determined by the integration of the quadrature given by Eq.(30), the cycles determines the polar angle as a function of the rotation angle  $\Theta$ ,

$$\cos \theta = \begin{cases} \cos \theta_{(-, -)} & 0 \leq \Theta \leq \Theta_0/2 \\ \cos \theta_{(-, +)} & \Theta_0/2 \leq \Theta \leq \Theta_0 \\ \cos \theta_{(+, -)} & \Theta_0 \leq \Theta \leq 3\Theta_0/2 \\ \cos \theta_{(+, +)} & 3\Theta_0/2 \leq \Theta \leq 2\Theta_0, \end{cases} \quad (48)$$

with period  $2\Theta_0$ . The polar angle ranges between a minimum  $\theta_{\text{Min}}$  (a maximum of  $\cos \theta$ ) and a maximum  $\pi - \theta_{\text{Min}}$ . The former is realized along the  $(+, +)$  segment, the latter along  $(-, +)$ . Each value of  $\theta$  describes a circular cone in Euclidean space centered on the torque axis. The spiral will thus nutate between two identical oppositely-oriented cones which bound the trajectory away from this axis.

The spiral will graze the bounding cones tangentially. These are *not* the turning points of the potential. Indeed the derivative  $d \cos \theta / dZ$  diverges at  $Z = Z_-$  and  $\text{Min}(Z_+, \gamma)$  (with  $d \cos \theta / dZ \sim 1/\sqrt{Z - Z_-}$  at  $Z_-$  and likewise); on taking the derivatives with respect to  $\Theta$  (or arc-length) these divergences multiply zeros ( $\sim \sqrt{Z - Z_-}$  and so on) originating in the multiplication by  $Z^\bullet$ . As a consequence,  $(\cos \theta)^\bullet$  is finite ( $\neq 0$ ) when  $Z$  coincides with a turning point of the potential. The bounding cones themselves will be examined more closely in section 5.1.

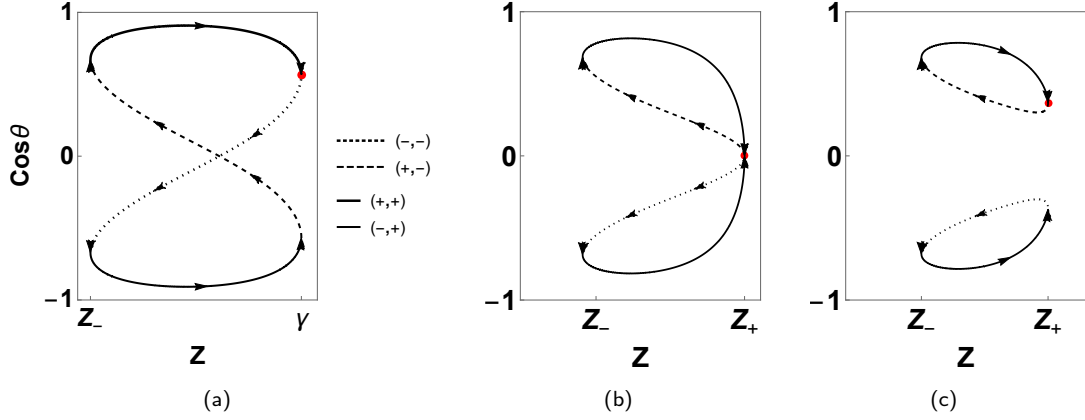


Figure 5: (a) Supercritical  $\cos \theta$  cycle ( $\gamma = 1.2, m = \sqrt{2}$ ); (b) Critical Cycle ( $\gamma = 1.2, m = 1.3$ ); (c) Subcritical cycle ( $\gamma = 1.2, m = 1.25$ ) and its reflected twin. The critical cycle occurs when  $m^2 = \gamma^3$  lying on the interface  $\mathcal{C}_1$  in parameter space (cf. Figure 3).

Supercritical cycles are symmetric under reflection in the mid plane:  $\theta \rightarrow \pi - \theta$ . However, the spiral trajectory itself is not. This is because it both precesses and expands as it nutates. In particular, the beginning and endpoints of the cycle never represent the same point in Euclidean space.

### Mid-plane crossings

The mid plane  $X_{\parallel} = 0$  (or  $\cos \theta = 0$ ) is crossed twice per cycle, once on the way down (with  $Z^{\bullet} < 0$ ) along the  $(-, -)$  cycle segment and again on the way up along the  $(+, -)$  segment. It is clear from Eq.(47) that this will occur when  $W_-(Z) = 0$ , or

$$(Z - Z_-)(Z_+ - Z) = Z(\gamma - Z). \quad (49)$$

This is a linear identity, and it is satisfied when  $Z = Z_{\theta=\pi/2}$ , where

$$Z_{\theta=\pi/2} = \gamma / [m^2 + 1 - \gamma^3]. \quad (50)$$

Here Eq.(26) has been used to express  $Z_-$  and  $Z_+$  in terms of  $\gamma$  and  $m$ .

It is simple to confirm that  $Z_{\theta=\pi/2}$  lies within the interval  $[Z_-, \gamma]$  if  $m^2 \geq \gamma^3$ . As  $m \rightarrow \infty$ ,  $Z_{\theta=\pi/2} \rightarrow Z_- \rightarrow 0$ . This behavior is displayed graphically in Figure 5.2(a).

**Aside on Subcritical Spirals:** If the spiral is subcritical,  $\tau$  has a fixed sign (say positive). Now  $\cos \theta$  is represented by two different functions of  $Z$ , one for each sign of  $Z^{\bullet}$ ,  $(+, -)$  and  $(+, +)$ . Their union forms a closed non-self intersecting loop on the  $(Z, \cos \theta)$  plane. A circuit of this cycle has a period  $\Theta_0$ . The cycle is represented by the upper loop in Figure 5(a) for  $\gamma = 1.2$  and  $m = 1.25$ .<sup>2</sup> Notice  $\cos \theta$  does not change sign; mid plane crossings do not occur. The angle  $\theta$  ranges between a positive minimum  $\theta_{\text{Min}}$  and maximum  $\theta_{\text{Max}} \leq \pi/2$ . The spiral will now nutate between the two cones defined by these angles. As  $m$  is lowered from  $\mathcal{C}_1$  towards  $\mathcal{C}_0$  for fixed  $\gamma$ , the cycles contract to a single point, representing the merger of the two cones, as illustrated in Figure 5 (c), into one.

If  $\gamma > 1$ , the supercritical figure of eight morphs discontinuously on reducing  $m$  into two disconnected, non-self-intersecting subcritical cycles as  $\mathcal{C}_1$  (cf Figure 3) is crossed. This behavior is displayed in the sequence (a-c) in Figure 5. The critical cycle with  $m^2 = \gamma^3$ , illustrated in the central panel, is singular if approached from either side. Mid-plane crossings do not occur in the limit  $m^2 \downarrow \gamma^3$ , because in this limit  $Z_{\theta=\pi/2} \uparrow \gamma$ , a double root of the potential with negative curvature, which is only reached asymptotically.

<sup>2</sup>The mirror image with respect to the mid-plane, with  $\tau < 0$ , represented by the  $(-, +)$  and  $(-, -)$  graphs describes a second disconnected spiral.

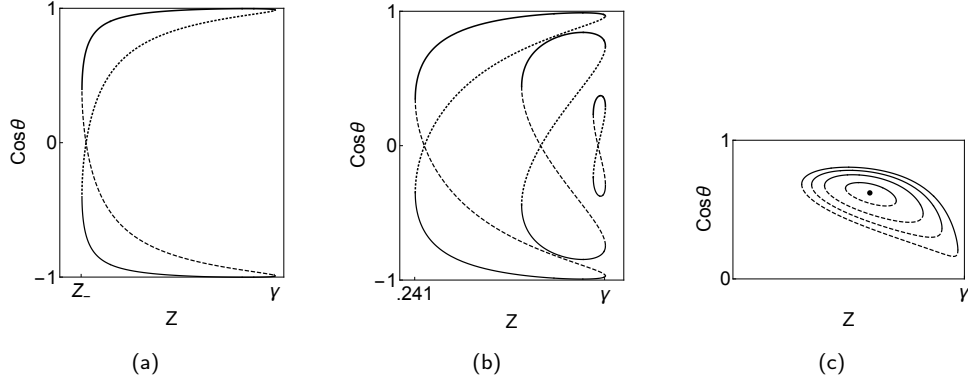


Figure 6: (a) Extremely asymmetric supercritical cycle ( $\gamma = 1.2, m = 3$ ); (b)  $\gamma < 1$  Sequence of supercritical cycles: ( $\gamma = 0.75, m = 1.5, 0.85, 0.67$ ). As  $m$  is lowered towards  $\gamma^3$ , the cycle vanishes; this contrasts with the behavior when  $\gamma > 1$ . As  $m$  increases the cycle grows both along  $Z$  and  $\theta_{\text{Min}} \rightarrow 0$ , in a manner qualitatively identical to (a); (c) Nested subcritical cycles ( $\gamma = 1.2, m = 1.31, 1.3, 1.29, 1.28$ ). As  $m$  tends towards its lower bound ( $C_0$ ), the cycles degenerate to a single point, representing a helix wound on a single cone with fixed  $Z$  and  $\theta$ , described in section Appendix B.

### Turning points of $X_{\parallel}$ in supercritical spirals do not occur on the bounding cones

Whereas the trajectory touches the two bounding cones tangentially, it intersects the turning cone at  $Z = \gamma$  with a non-vanishing angle of incidence. At the extrema of  $X_{\parallel}$ ,  $Z = \gamma$ , so Eq.(47) implies that  $\cos \theta$  assumes the value

$$\cos \theta_{\gamma} = \pm \sqrt{\frac{m^2 + 1}{m^2}} \sqrt{1 - \frac{\gamma^3}{m^2}} / \sqrt{1 - \frac{\gamma^3}{m^2 + 1}}. \quad (51)$$

Evidently  $\theta_{\gamma} > \theta_{\text{Min}}$  (cf. Figure 7). If  $m$  is large,  $\theta_{\gamma} \approx 0$ , and with it goes  $\theta_{\text{Min}}$ . The trajectory is freed to range through three-dimensional space. The excluded region disappears.

Along the cycle,  $\theta = \theta_{\gamma}$  at two different values of  $Z$ , once at  $Z = \gamma$  but also again at another lower value,  $Z_{\gamma 1}$  say.  $Z_{\gamma 1}$  is not, however a local maximum of  $X_{\parallel}$  and the torsion does not vanish there. In an expanding spiral, the  $\theta_{\gamma}$  cone is always entered when  $Z = Z_{\gamma 1}$ , and exited with  $Z = \gamma$  (the red point in Figure 5(a)). Along which cycle segment entry occurs will depend on the relative values of the cosine at  $Z_{-}$  and  $Z_{\gamma 1}$ , which depends on the value of  $m$  (cf. Figure 7). The spiral geometry is asymmetric with respect to exit and re-entry of this cone. Between entry and exit  $X_{\parallel}$  increases (if positive), reaching a local maximum upon exit where the torsion vanishes and changes sign; in its sojourn with this cone the trajectory grazes the interior bounding cone with  $\theta = \theta_{\text{Min}}$  once.

It is also evident from inspection of Eq.(43) that the fastest ascent always occurs at  $Z_{-}$  (in subcritical trajectories the slowest ascent occurs at  $Z_{+}$ ). It may seem surprising that this not occur where the trajectory crosses the mid plane, but not if one recalls that the trajectory is not symmetric with respect to reflection in this plane. The angle  $\Psi$  that the tangent makes with  $\mathbf{M}$  (cf. Eq.(42)) is minimized at this value of  $Z$ :  $\cos \Psi = \pm (2\gamma^3 / [m^2 + 1 - \sqrt{(m^2 + 1)^2 - 4\gamma^3}] - 1)^{1/2} / m$ . As  $m \rightarrow \infty$ , for fixed  $\gamma$ ,  $\cos \Psi_{\text{max}} \rightarrow 1$  independent of  $\gamma$ . Yet there is no finite critical value above which  $\mathbf{t}$  is aligned or anti-aligned with  $\mathbf{M}$ .

If  $m$  is increased for fixed  $\gamma$ , the cycle becomes increasingly asymmetric with  $\theta_{\gamma} \rightarrow 0$  and  $\theta_{\text{Min}} \rightarrow 0$ . We note, however, that  $\theta$  is never strictly 0 or  $\pi$  unless in the limit  $m \rightarrow \infty$ , though it does get very close at even modest values. This behavior is displayed in Figure 5(a) for  $\gamma = 1.2$ , and again in Figure 6(b) for  $\gamma < 1$ . It is observed that the area enclosed by the large  $m$  limiting cycles tends to zero. It is not clear if this area itself possesses geometrical significance.

The simple global identity  $\oint d\theta \tau / \kappa = \int ds \tau = 0$  is satisfied along all supercritical cycles. Along subcritical cycles, it assumes a non-vanishing value. But each cycle contributes equally so that the total torsion is infinite along the entire

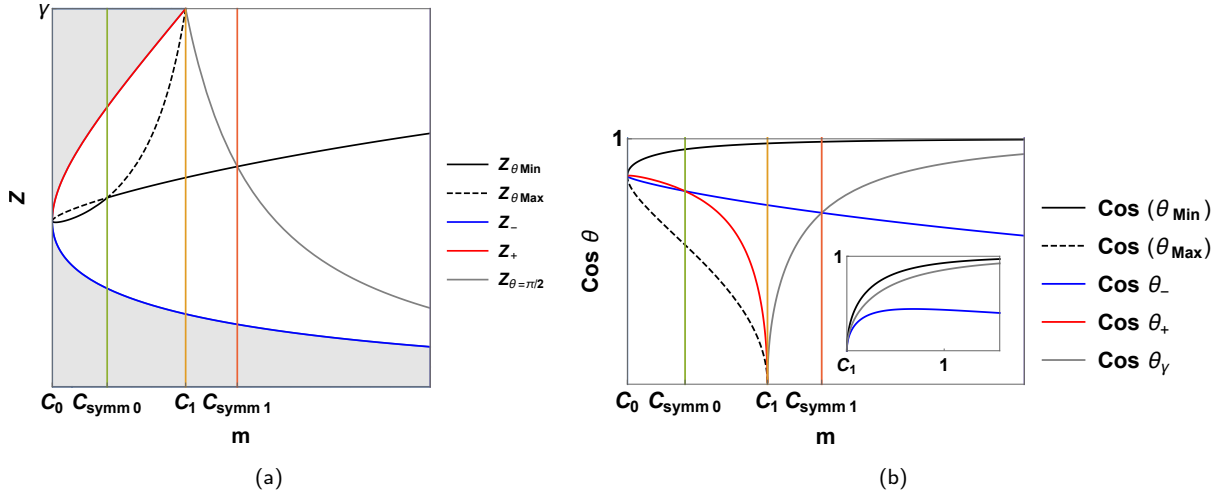


Figure 7: (a) Locating  $Z$  where  $\theta = \theta_{\text{Min}}$  as a function of  $m$  ( $\gamma = \sqrt{3}$ ); and below  $C_1$ , where  $\theta = \theta_{\text{Max}}$ ; (b) The corresponding apex angle cosines of the bounding cones; the insert reveals the very different behavior of  $\theta$  when  $\gamma < 1$  (here  $\gamma = 0.75$ ). The values of  $Z_-$  and  $\text{Min}[Z_+, \gamma]$  and the corresponding cosines are included (in blue and red) for reference.

spiral.

## 5.1 Locating the bounding cones

It is instructive to examine how the opening angles of the bounding cones vary across parameter space. Using Eq.(47) with  $W_{\pm}$  defined by Eq.(40), it is evident that  $\theta_{\text{Min}}$  is always located where  $dW_+/dZ = 0$ ; in a subcritical spiral, the maximum in a subcritical cycle  $\theta_{\text{Max}}$  occurs when  $dW_-/dZ = 0$ . In Appendix C, it is shown that  $dW_{\pm}/dZ = 0$  when

$$[\gamma^6 + 4\gamma^3 - (m^2 + 1)^2]Z^2 + \gamma[(m^2 + 1)(m^2 + 1 - \gamma^3) - 4\gamma^3]Z + \gamma^5 = 0. \quad (52)$$

The two roots are given by

$$Z_{\theta 1,2}/\gamma = \frac{-[(m^2 + 1)(m^2 + 1 - \gamma^3) - 4\gamma^3] \pm \sqrt{-(1 - \gamma^3 + m^2)^2(4\gamma^3 - (1 + m^2)^2)}}{2[\gamma^6 + 4\gamma^3 - (m^2 + 1)^2]}. \quad (53)$$

The opening angle  $\theta_{\text{Min}}$  occurs at the smaller root  $Z_{\theta \text{ Min}}$  of the quadratic, given by Eq.(52). The dependence of  $Z_{\theta \text{ Min}}$  and  $\cos(\theta_{\text{Min}})$  on  $m$  for a fixed value of  $\gamma$  is indicated by the solid black curves in Figures 7(a) and 7(b).

In subcritical spirals the two roots lie within the interval  $[Z_-, Z_+]$ ; the larger root identifies the opening angle of the exterior bounding cone,  $\theta_{\text{Max}}$ . The dependence of  $Z_{\theta \text{ Max}}$  and  $\cos(\theta_{\text{Max}})$  on  $m$  for a fixed value of  $\gamma$  is indicated by the dashed black curves in Figure 7. The minimum, as was seen, occurs along the  $(+, +)$  cycle segment, the maximum along  $(+, -)$ . The values of  $Z$  coincide, or  $Z_{\theta \text{ Min}} = Z_{\theta \text{ Max}}$ , when the discriminant on the right in Eq.(53) vanishes. This occurs either trivially if  $(m^2 + 1)^2 = 4\gamma^3$ , or, non-trivially if  $m^2 = \gamma^3 - 1$ . The former corresponds to the collapse of the Cosine cycle to a single point along the interface  $C_0$  in parameter space, so that  $\theta_{\text{Max}} = \theta_{\text{Min}}$  and the two bounding cones coincide. The non-trivial possibility, with  $\theta_{\text{Max}} \neq \theta_{\text{Min}}$  is consistent with the lower bound on  $m$  only when  $\gamma^3 \geq 4$ . The corresponding locus in parameter space is indicated by the curve  $C_{S0}$  in Figure 8. The  $\cos \theta$  cycle exhibits a left-right symmetry where this occurs.

In supercritical spirals (above  $C_1$ ) the larger root of the quadratic, given by (53), lies outside the interval  $[Z_-, \gamma]$ . Even though it lies outside the well it still conveys information concerning behavior within it. In particular, it diverges when the coefficient  $a = (m^2 + 1)^2 - 4\gamma^3 - \gamma^6$  in the quadratic term in (52) vanishes indicating its reduction to a linear equation, possible only if the spiral is supercritical. This value of  $m$  locates  $Z_{\theta \text{ min}}$  at  $Z_{\theta=0}$ . When this occurs, the  $\cos \theta$  cycle is again left-right symmetric about this value of  $Z$ . The corresponding locus in parameter space is indicated by the curve  $C_{S1}$  in Figure 8. This curve lies above  $C_1$  in the admissible region, intersecting it when  $\gamma^3 = 1/2$ . This



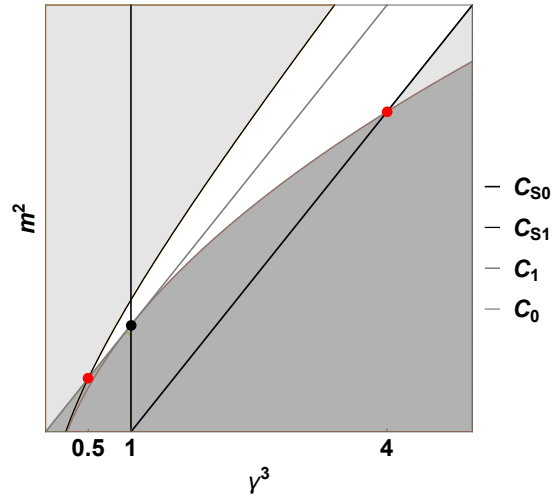


Figure 8:  $\mathcal{C}_{S0}$  ( $\mathcal{C}_{S1}$ ) locates symmetric subcritical (supercritical) cosine cycles in parameter space. Below  $\gamma^3 = 4$ , all non-conical subcritical cycles are asymmetric; below  $\gamma^3 = 0.5$ , all cycles are asymmetric.

indicates that there are no symmetric supercritical cycles if  $\gamma^3 < 1/2$ .

In Figure 7(b), observe that  $\theta_{\text{Min}}$  is continuous as a function of  $m$  across  $\mathcal{C}_1$ ; while  $\theta_{\text{Max}} \uparrow \pi/2$  as  $m^2 \uparrow \gamma^3$ , and  $\theta_\gamma \uparrow \pi/2$  as  $m^2 \downarrow \gamma^3$ . These results are consistent with the limiting asymptotically planar logarithmic spiral form as  $\mathcal{C}_1$  is approached from above and below when  $\gamma > 1$  discussed in section 3.3. Above  $\mathcal{C}_1$ ,  $\theta_\gamma$  decreases monotonically to zero from  $\pi/2$ . The position of  $Z_{\theta=\pi/2}$ , locating mid-plane crossing (discussed in section 5), is indicated by the descending gray curve in Figure 7(a). It originates at  $Z = \gamma$  along  $\mathcal{C}_1$  and is always bounded below by  $Z_-$ .

As  $m$  is increased further, as illustrated in Figure 7, all cycles tend to a qualitatively identical form with  $\theta_{\text{Min}}$  and  $\theta_\gamma \rightarrow 0$  as the two cones close onto the pole;  $\theta_{Z_-}$  however decreases monotonically to  $\pi/2$ , while the range of  $Z$  approaches its maximum extent,  $[0, \gamma]$ . This asymmetry in the corresponding cycles is illustrated in Figure 5(a), as well as the left-most cycle in (b).

The insert in Figure 7(b), describing  $\gamma < 1$  supercritical cycles, indicates that  $\theta_{\text{Min}} = \pi/2$  along  $\mathcal{C}_1$  so that cycles vanish there. The vanishing point represents a logarithmic spiral. The distinction between limiting supercritical spirals with  $\gamma < 1$  and  $\gamma > 1$  from the point of view of their bounding cones will be examined in section 5.3.

## 5.2 Cone closure

Just how rapidly  $\theta_{\text{Min}} \rightarrow 0$  as  $m$  increases can be best appreciated by examining a contour of constant  $\theta_{\text{Min}}$  in parameter space. In Figure 9 these contours are represented for a sequence of very small conical opening angles. Panel (a) in this figure indicates that spiral trajectories describing *small* deviations of a planar logarithmic spiral (say even  $\theta_{\text{Min}} = \pi/3$ ) are confined within a very narrow sliver of parameter space extending from the origin to the point  $(1, 1)$ .

In section 10, we will illustrate how the closure of the limiting cones on the spiral trajectory facilitates its passage through its three-dimensional environment.

## 5.3 Limiting Supercritical spirals

In the neighborhood of the interface  $\mathcal{C}_1$  in parameter space the behavior of  $\theta_{\text{Min}}$  in supercritical spirals in the regime  $\gamma < 1$  contrasts significantly with that in the regime  $\gamma > 1$ . Let  $m^2 = \gamma^3 + \delta m^2$ , where  $\delta m^2$  is small. In the case  $\gamma < 1$ , as shown at the very end of section 3.3,  $Z_- \approx \gamma - 2\gamma\delta m^2/(1 - \gamma^3)$ . In the quadratic approximation, the

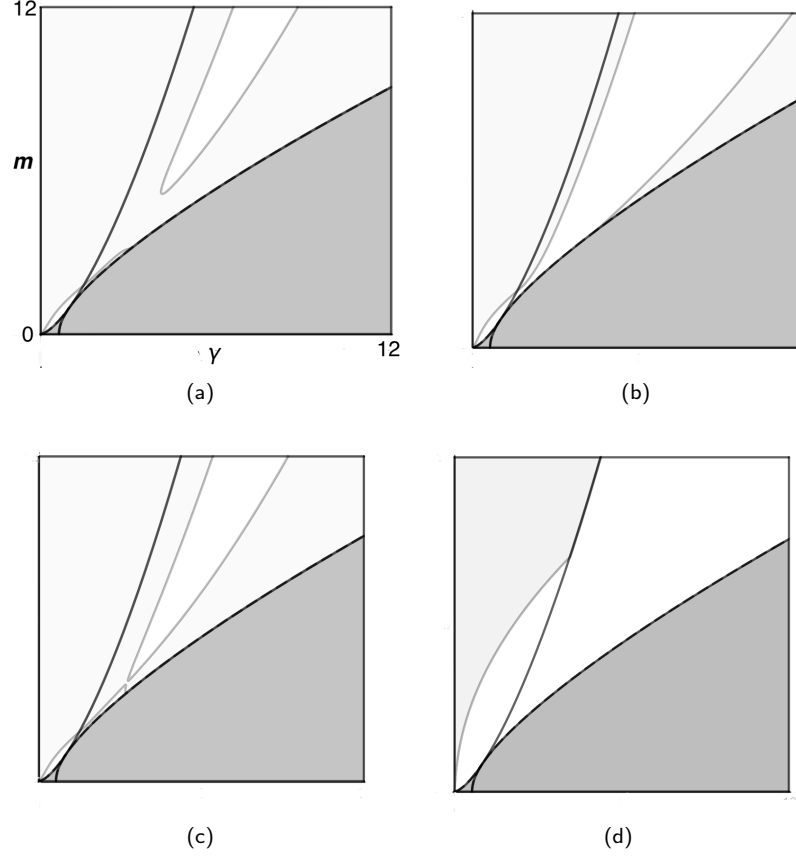


Figure 9:  $(\gamma, m)$  parameter space with contours of constant  $\cos(\theta_{\text{Min}}) = 0.95, 0.9529, 0.97$  and  $0.9999$  (a-d), on same scale. The white (light gray) region indicates where  $\cos(\theta_{\text{Min}})$  is lower (greater) than the indicated value; the dark gray region is forbidden. Notice that  $\cos(\theta_{\text{Min}}) \geq 0.95$  over a large expanse of parameter space, both subcritical and supercritical. Indeed, all supercritical spirals outside a narrow bend terminating just above  $\gamma = 1$  possess a vanishingly small opening angle; witness what occurs when the cosine is raised to  $0.9999$ . It is also evident that these contours reveal a number of intriguing unanticipated complex patterns worthy of closer examination but beyond the scope of this paper.

quadrature describing the small well lying between  $Z_-$  and  $\gamma$  is given by

$$\frac{1}{4}Z^2 - (1 - \gamma^3)(\gamma - Z) \left( Z - \gamma + \frac{2\gamma\delta m^2}{1 - \gamma^3} \right) = 0. \quad (54)$$

The motion in this well is harmonic in  $\Theta$ ,

$$\gamma - Z = \frac{\gamma\delta m^2}{1 - \gamma^3} (1 - \cos \omega \Theta) = 0, \quad (55)$$

where  $\omega = 2\sqrt{1 - \gamma^3}$  is the curvature of the potential at  $Z = \gamma$  in this limit. The period of oscillations in the vanishing small well remains finite (just as it does in deformed conical helices) so long as  $\gamma \neq 1$ . In this limit, it is possible to approximate  $\cos \theta$ , given by Eq.(47) to first order in  $\delta m^2$ :

$$\cos \theta \approx \frac{1 + \gamma^3}{1 - \gamma^3} (1 - \cos \omega \Theta) \delta m^2, \quad (56)$$

with a maximum linear in  $\delta m^2$ , with proportionality,  $2(1 + \gamma^3)/(1 - \gamma^3)$ . We notice that perturbation theory breaks down as the critical point  $\gamma = 1 = m$  is approached. Away from this point, Eq.(56) describes small *symmetric* oscillations about a logarithmic spiral. It would be interesting to compare observed non-planar *logarithmic* patterns

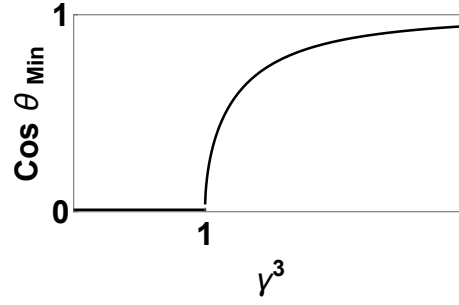


Figure 10:  $\cos(\theta_{\text{Min}})$  vs.  $\gamma$  along the boundary  $\mathcal{C}_1$ . The details in the immediate vicinity of  $\gamma = 1$  require a more careful (non-perturbative) treatment than the one sketched here.

in the arms of spiral galaxies with these templates.

If, on the other hand,  $\gamma > 1$ , then  $Z_- = 1/\gamma^2$ , while  $Z_+ \downarrow \gamma$ . and there are no small *symmetrical* excursions about logarithmic spirals. The minimum conical angle  $\theta_{\text{Min}}$  is bounded away from  $\pi/2$  for each value of  $\gamma$ , consistent with the continuity of  $\theta_{\text{Min}}$  across  $\mathcal{C}_1$ , as illustrated in Figure 7.

A plot of  $\theta_{\text{Min}}$  vs.  $\gamma$  along the boundary  $\mathcal{C}_1$  is provided in Figure 10. At lowest order,  $Z_+ = \gamma$ . The minimum  $\theta_{\text{Min}}$  occurs where  $Z$  satisfies Eq.(52), with  $m^2 = \gamma^3$ , which reduces to <sup>3</sup>

$$Z_{\text{Min}} = \frac{\gamma^4}{2\gamma^3 - 1}, \quad (57)$$

and

$$\cos(\theta_{\text{Min}}) = \sqrt{1 - \gamma^{-6}}. \quad (58)$$

## 6 The distance to the apex increases monotonically

Intuitively, the distance to the apex  $\rho$  is expected to increase monotonically with arc-length  $s$ . Yet it is also known that  $X_{\parallel}$  oscillates in supercritical spirals: so it is worth confirming that this intuition is sound. As a bonus, a simple and useful identity for  $\rho'$  is revealed.

First rewrite Eq.(45) in the form

$$(m^2 + 1)\rho^2 = m^2 X_{\parallel}^2 + \frac{\gamma}{\kappa^2 Z}. \quad (59)$$

Now

$$(m^2 + 1)\rho\rho^{\bullet} = m^2 X_{\parallel} X_{\parallel}^{\bullet} - \frac{\gamma}{\kappa^2} \frac{Z^{\bullet}}{2Z^2} + \frac{\gamma Z^{1/2}}{\kappa^2} = \frac{\gamma^2}{\kappa^2 Z^{1/2}}. \quad (60)$$

Use has been made of the identities (39) and (43) for  $X_{\parallel}$  and its derivative, as well the quadrature (23) to eliminate  $Z^{\bullet}$  in terms of  $Z$  (modulo  $\text{sign}(Z^{\bullet})$ ), and the definition of  $Z$  through  $\Sigma$  to connect  $\kappa^{\bullet}$  to  $Z^{\bullet}$ . The final expression in Eq.(60) is manifestly positive confirming that  $\rho$  increases monotonically everywhere. The simple identity for the dimensionless  $\rho'$ ,

$$\rho'^2 = \frac{\gamma^3}{m^2 + 1} \frac{1}{1 + \gamma W_{\pm}(Z)^2} \quad (61)$$

follows ( $W_{\pm}$  was defined in Eq.(40)). Along a conical helix,  $Q = 0$ , and  $Z = \gamma^{-1/2}$ , which reproduces the result  $\rho' = 1/\sqrt{2}$  derived in Appendix B.

In Appendix D, it is shown that a sharp upper bound can be placed on  $\rho'$ , bounding it strictly below 1, the Euclidean

<sup>3</sup>The second root at  $Z = \gamma$  is spurious. It corresponds to the location of  $\theta_{\text{Max}}$  in the limit  $m^2 \uparrow \gamma^3$ .

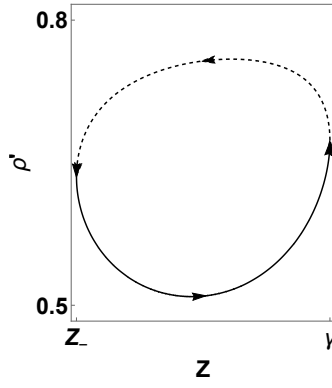


Figure 11: A supercritical  $\rho'$  cycle ( $\gamma = 1.2$ ,  $m = \sqrt{2}$ ).  $\rho$  increases most rapidly outside the  $\theta_\gamma$  cone, and most slowly within it close to the bounding cone.

limit. Sharp lower bounds guaranteeing strict monotonicity can also be established. These bounds are captured in the cyclic behavior of  $\rho'$ , illustrated for  $\gamma = 1.2$  and  $m = \sqrt{2}$  in Fig. 11. An immediate but nevertheless important consequence of the monotonicity of  $\rho$  is that the spiral geometry never exhibits *accidental* self-intersections. As such, knotted self-similar spirals do not exist.

To determine  $\rho$  as a function of  $\Theta$  one can either integrate the  $\rho'$  cycle given by (61) or use the cyclical variable  $\kappa\rho$  given by Eq.(45), modulated by the falloff in  $\kappa$  given by Eq.(31):

$$\rho = \begin{cases} (\kappa\rho)_-/\kappa, & 0 \leq \Theta \leq \Theta_0/2 \\ (\kappa\rho)_+/\kappa, & \Theta_0/2 \leq \Theta \leq \Theta_0. \end{cases} \quad (62)$$

To complete the determination of  $\rho$  along the second half-cycle, Eq.(62) is modified with the appropriate continuation of Eq.(31) for  $\kappa$ .

## 7 $X_\perp$ is not monotonic if $m$ is large

Just as  $X_\parallel$  oscillates in supercritical spirals, if  $m$  is sufficiently large the perpendicular distance from the torque axis  $X_\perp$  ceases to behave in a monotonic manner. But this can occur in both subcritical and supercritical spirals.

The Pythagorean decomposition of  $\rho^2$  in terms of  $X_\parallel^2$  and  $X_\perp^2$  implies

$$\rho\rho' = X_\perp X'_\perp + X_\parallel X'_\parallel, \quad (63)$$

so that

$$\sin\theta X'_\perp = \rho' - \cos\theta X'_\parallel. \quad (64)$$

It is evident that  $X'_\perp$  is not necessarily positive; it vanishes whenever  $\rho' = \cos\theta X'_\parallel$ , or

$$(m^2 + 1)QT = Z^{1/2}((m^2 + 1)Z - \gamma), \quad (65)$$

and  $Z^\bullet > 0$ , where the identity (63) is used to eliminate  $\rho'$ , the expressions (43) for  $X'_\parallel$  and (47) for the cosine, as well as the definition Eq.(40). In general,

$$\begin{aligned} (m^2 + 1)m^2(\kappa X_\perp)X'_\perp &= \frac{\gamma}{Z} \left[ -(m^2 + 1)\text{sign}(Z^\bullet)Q(\gamma - Z)^{1/2} \right. \\ &\quad \left. + Z^{1/2}((m^2 + 1)Z - \gamma) \right], \end{aligned} \quad (66)$$

independent of the sign of  $\tau$ . Evidently,  $X'_\perp$  forms a cycle. If  $X'_\perp$  is negative it can only occur along the  $(+, +)$  and  $(-, +)$  cycle segments. The supercritical cycle corresponding to the parameter values  $\gamma = .75$ ,  $m = .85$  is presented

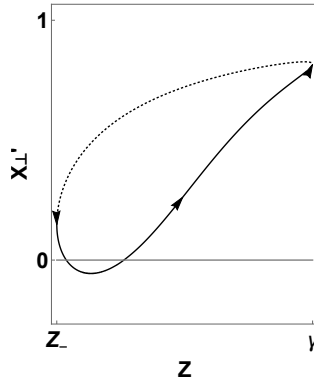


Figure 12: Supercritical  $X'_\perp$  cycle ( $\gamma = 0.75$ ,  $m = 0.85$ ).  $X'_\perp$  is negative along connected segments of the  $(+, +)$  and  $(-, +)$  quarter cycles. The length of these segments increases monotonically as  $m$  is increased.

in Figure 12; its period is  $\Theta_0$ .

Eq.(65) can be cast as a quadratic in  $Z$ :

$$\frac{m^2 + 1}{\gamma^2}[(m^2 + 1)^2 + (m^2 - 1)\gamma^3]Z^2 - \frac{1}{\gamma}[(m^2 + 1)^3 + (m^2 + 1)^2 - \gamma^3]Z + (m^2 + 1)^2 = 0. \quad (67)$$

The quadratic possesses two real roots whenever the discriminant

$$D = \gamma^6 - 2m^2(1 + 2m^2)(m^2 + 1)^2 + m^4(m^2 + 1)^4 \quad (68)$$

is not negative, or

$$1 + 4m^2 + 5m^4 + 2m^6 + 2\sqrt{m^2(1 + m^2)^5} \geq \gamma^3/m^2. \quad (69)$$

The region in parameter space where  $D > 0$  is indicated in light gray in Figure 13. If  $\gamma$  is fixed and  $m$  is large enough,  $X_\perp$  is not a monotonic function of  $s$ . Surprisingly, monotonic behavior occurs only within a narrow band of values of  $m$ .

Supercritical deformations of logarithmic spirals with  $\gamma < 1$  exhibit monotonicity if  $m$  is not too large consistent with their interpretation as small deformations of logarithmic spirals. This pattern is followed above  $\gamma = 1$  until a critical value of  $\gamma$  is reached ( $\gamma^3 = 2.38298$  or  $\gamma^{1/3} = (54 - 6\sqrt{33})^{1/3} + (2(9 + \sqrt{33}))^{1/3}/3^{2/3}$ ) even though these spirals cannot in any sense be considered deformations of logarithmic spirals; above this value all supercritical spirals exhibit oscillations in  $X_\perp$ . This critical value is indicated by the red point in Figure 13. Below this value, on the other hand,  $X_\perp$  is monotonic in all subcritical spirals; above it monotonic behavior occurs only in ever smaller deformations of conical spirals.

When  $D > 0$ , the two real roots of the quadratic (67) are given by

$$Z_{0 \text{ Min, Max}}/\gamma = \frac{2 - \gamma^3 + m^2(5 + 4m^2 + m^4) \pm \sqrt{\gamma^6 - 2\gamma^3 m^2(1 + 2m^2)(m^2 + 1)^2 + m^4(m^2 + 1)^4}}{2(1 - \gamma^3 + 3m^2(m^2 + 1) + \gamma^3 m^4 + m^6)}. \quad (70)$$

It is easy to confirm that they both lie within the accessible region  $[Z_-, \text{Min}(Z_+, \gamma)]$ . Their behavior for fixed  $\gamma = 0.8$  as a function of  $m$  is displayed in Figure 14.

Eq.(64) reveals that  $X'_\perp = 0$  never occurs on the mid-plane. In addition, the extrema of  $\theta$  and  $X_\perp$  never coincide (unless asymptotically in  $m$ ). This is because the extrema of  $\cos \theta = X_\parallel/\rho$  occur when  $\cos \theta = X'_\parallel/\rho'$ . This feature is evident in Figure 14.

Even though it is not generally monotonic,  $X_\perp$  never returns to zero if  $\gamma$  or  $m$  is finite. On the other hand, as has been seen, with even modestly large values of  $m$  the bounding cones close down with  $\theta_{\text{Min}} \approx 0$  and with it  $X_{\perp \text{ Min}} \approx 0$ , so that the spiral trajectory visits the polar neighborhoods in every cycle.

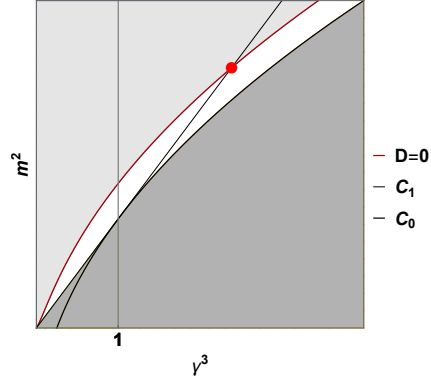


Figure 13: The contour  $D = 0$ , indicating the trajectory in parameter space separating monotonic and non-monotonic behavior of  $X_\perp$ ; in the white region  $D < 0$ , and  $X_\perp$  is monotonic; in the region shaded light gray,  $X_\perp$  is not monotonic.

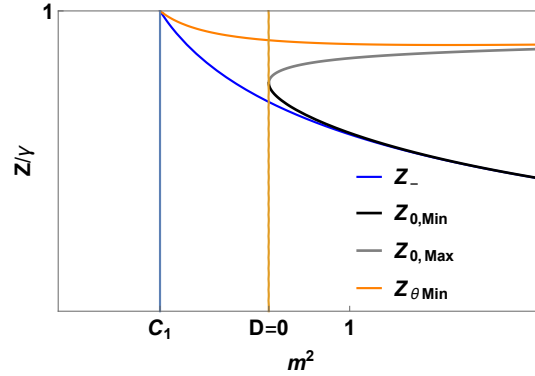


Figure 14:  $Z_{0,Min}$  (black) and  $Z_{0,Max}$  (gray) as functions of  $m$  for  $\gamma = 0.8$ . Thus  $X'_\perp < 0$  for all values of  $Z$  within the band  $[Z_{0,Min}, Z_{0,Max}]$  along the  $(+, +)$  and  $(-, +)$  Cosine quarter cycles. We note that this band lies below  $Z_{\theta,Min}$ , the value of  $Z$  where  $\theta_{Min}$  is achieved, and above  $Z_-$ . As  $m$  increases, however, the band extends from  $Z_- \rightarrow 0$  to  $Z_{\theta,Min} \rightarrow \gamma$ . In other words,  $X_\perp$  is then decreasing along half of each cycle.

## 8 The azimuthal advance and spiral precession

There remains to determine the azimuthal progress of the spiral. One way to do this is the obvious one: integrate the arc length identity  $\rho'^2 + \rho^2(\theta'^2 + \sin^2 \theta \phi'^2) = 1$ , using the expressions (45) for  $\rho$  and (47) for  $\theta$ , or the equivalent expression for  $X_{\parallel}$  and  $X_{\perp}$  in cylindrical polars. However, a more direct and transparent expression for  $\phi'$  is implied by the conservation of the special conformal current.

### A vector orthogonal to the spiral position with respect to its apex

The projections of Eq.(36) along  $\mathbf{X}$  and orthogonal to it have been used to identify  $\rho$  and  $\cos \theta$ . Taking its projection along  $\mathbf{t}$ , one obtains the identity

$$\mathbf{X} \cdot (\mathbf{t} \times \mathbf{M}) + S(\mathbf{X} \cdot \mathbf{t}) = 0; \quad (71)$$

as a consequence the vector

$$\mathbf{J} = \mathbf{t} \times \mathbf{M} + S\mathbf{t} = [\mathbf{X} \times \mathbf{M} + S\mathbf{X}]' \quad (72)$$

is orthogonal to  $\mathbf{X}$  at every point along the tension-free spiral trajectory:  $\mathbf{X} \cdot \mathbf{J} = 0$ . The vector  $\mathbf{J}$  itself is not conserved.<sup>4</sup> Using the expression (5) for  $\mathbf{M}$ , it is possible to cast  $\mathbf{J} = H_1 \mathbf{N} - H_2 \mathbf{B} - S\mathbf{t}$ . The identity  $\mathbf{X} \cdot \mathbf{J} = 0$  can then be read as a homogeneous constraint on the projections of  $\mathbf{X}$  onto the Frenet frame. This may be interesting but it is not the direction we will take.

More immediately relevant is the fact that the condition  $\mathbf{X} \cdot \mathbf{J} = 0$  determines  $\phi'$  in terms of  $\rho$ ,  $\rho'$  and  $\theta$ . To see this write Eq.(72) in the equivalent form,

$$\mathbf{X} \cdot \mathbf{J} = -S|\mathbf{X}|^2/2 + \mathbf{t} \cdot \mathbf{X} \times \hat{\mathbf{M}} = 0. \quad (73)$$

This identity can be recast in terms of the spherical polar coordinates adapted to the torque vector:

$$\rho' = m\rho \sin^2 \theta \phi'. \quad (74)$$

Because  $\kappa\rho$ ,  $\rho'$  and  $X'_{\parallel}$  form periodic cycles, it is now evident that both  $\phi^{\bullet}$  as well as the orbital velocity  $X_{\perp}\phi'$  about  $\mathbf{M}$  do also. To derive Eq.(74), decompose  $\mathbf{t}$  with respect to the associated orthonormal frame :  $\mathbf{t} = \rho'\hat{\mathbf{X}} + \rho\phi'\sin\theta\hat{\boldsymbol{\phi}} + \rho\theta'\hat{\boldsymbol{\theta}}$ , so that

$$\mathbf{t} \times \hat{\mathbf{X}} = -\rho\sin\theta\phi'\hat{\boldsymbol{\theta}} + \rho\theta'\hat{\boldsymbol{\phi}}; \quad (75)$$

upon substitution into Eq.(73), the identity (74) follows. Notice the consistency of Eq.(74) with Eq.(B.6) which applies to conical helices where both  $\rho'$  and  $\theta$  are constant. A significant consequence of Eq.(74) is that  $\phi' > 0$ :  $\phi$  thus increases monotonically with  $s$ . There are no spiral switchbacks.

$\phi^{\bullet}$  and  $X_{\perp}\phi'$  cycles are illustrated in Figure 15.

Integrating Eq.(74) for each of the signs of  $Z^{\bullet}$ ,

$$\begin{aligned} \phi_{\pm} &= \frac{1}{m} \int d\Theta \frac{\rho'}{\kappa\rho \sin^2 \theta} \\ &= \frac{\gamma}{m} \int d\Theta \frac{Z^{1/2}}{1 - \gamma m^{-2} W_{\pm}(Z)^2}, \end{aligned} \quad (76)$$

where Eqs.(45) and (61), as well as the identity (47) implying

$$\sin \theta_{\pm} = \sqrt{\frac{1 - \gamma m^{-2} W_{\pm}(Z)^2}{1 + \gamma W_{\pm}(Z)^2}}, \quad (77)$$

---

<sup>4</sup>Its projection along  $\mathbf{t}$  is conserved.

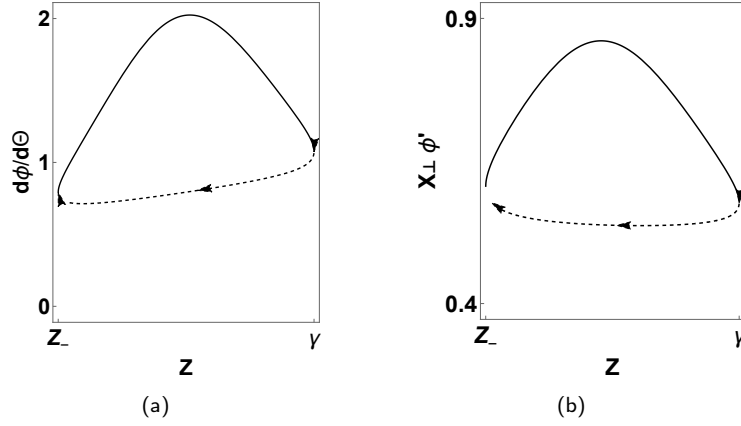


Figure 15: (a)  $\phi^\bullet$  cycle; (b)  $X_\perp \phi'$  cycle (both for  $\gamma = 1.2$ ,  $m = \sqrt{2}$ ).  $\phi$  evidently advances most rapidly along the  $(+, +)$  and  $(-, +)$  cycle segments close to the bounding cones.

are used on the second line. The integrand in Eq.(76) is a function of  $Z$ . Using the quadrature,  $\phi$  can be expressed as a function of  $\Theta$ . If  $\phi(0) = 0$ , the advance of the azimuthal angle over a complete supercritical cycle is given by

$$\phi = \begin{cases} \phi_-(\Theta) & 0 \leq \Theta \leq \Theta_0/2 \\ \phi(\Theta_0/2) + \phi_+(\Theta) & \Theta_0/2 \leq \Theta \leq \Theta_0 \\ \phi(\Theta_0) + \phi_-(\Theta) & \Theta_0 \leq \Theta \leq 3\Theta_0/2 \\ \phi(3\Theta_0/2) + \phi_+(\Theta) & 3\Theta_0/2 \leq \Theta \leq 2\Theta_0, \end{cases} \quad (78)$$

where  $\phi_\pm$  is given by Eq.(76) with the initializations indicated on the right. On completing the cycle, the spiral has undergone a rotation about the torque axis by the constant value

$$\phi_0 = \frac{2\gamma}{m} \int_0^{\Theta_0} d\Theta Z^{1/2} \left( \frac{1}{1 - \gamma m^{-2} W_-(Z)^2} + \frac{1}{1 - \gamma m^{-2} W_+(Z)^2} \right). \quad (79)$$

In general, Eq.(76) implies that

$$\phi(\Theta + \Theta_0) = \phi(\Theta) + \phi_0/2; \quad (80)$$

$\phi_0 = \phi(\Theta_0)$  is generally not proportional to  $\Theta_0$ . Although the local precession is not uniform within individual cycles, the cycles themselves precess uniformly. In any case, the precession depends only on  $\Theta$ , and not explicitly on arc length  $s$ .

Upper and lower bounds on  $W_\pm$  can be used to bound  $\phi$  as a function of  $\Theta$ . It is simple to see that  $\phi_0 \geq 2\Theta_0$ . But  $\phi_0$  never significantly exceeds  $2\Theta_0$ . The observed pattern of cycle nutation and precession can be attributed to this *coincidence*. This bound is saturated along  $\mathcal{C}_1$  ( $m^2 = \gamma^3$ ) when  $\gamma < 1$ . For now  $Z \approx \gamma$  and  $W_\pm = 0$ , so that  $\phi_0 = 2\Theta_0$ , an unexpected coincidence. Moreover  $\Theta_0 = 1/\sqrt{1 - \gamma^3}$ , a value completely determined by the curvature of the potential at  $Z = \gamma$ , given by Eq.(54).

In Figure 16  $\phi_0$  and  $2\Theta_0$  are plotted as functions of  $m$  for two different fixed values of  $\gamma < 1$ .

If  $\gamma > 1$ , and  $m^2 \approx \gamma^3$  either above it or below,  $\Theta_0$  diverges (this is because the curvature of the potential at  $Z = \gamma$  is negative). The integrands appearing on the right in Eq.(79), nevertheless, remain finite along the cycle; thus  $\phi_0$  also diverges while the ratio  $\phi_0/(2\Theta_0)$  remains finite. Its value depends on the value of  $\gamma$ .



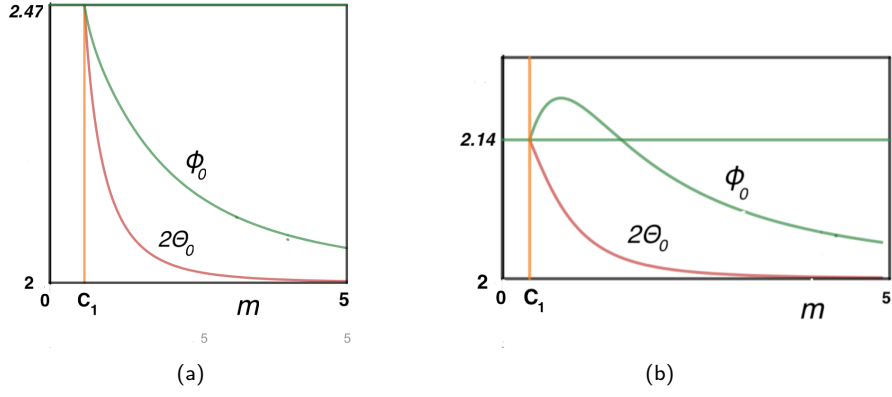


Figure 16:  $\phi_0/\pi$  (green) and  $2\Theta_0/\pi$  (red) vs.  $m$  for  $\gamma < 1$  (a)  $\gamma = 0.7$ ,  $m \in [0.7^{3/2}, 5]$ , (b)  $\gamma = 0.5$ ,  $m \in [(0.5)^{3/2}, 4]$ . Notice that  $\phi_0 \geq 2\Theta_0$ , with equality along  $C_1$  where  $m^2 = \gamma^3$ . Above  $C_1$ ,  $\Theta_0$  decreases monotonically to  $2\pi$ ;  $\phi_0$  does as well if  $4\gamma^3 > 1$  (realized in (a)), but does not below this value (b) (it increases initially before beginning its slow descent towards  $2\pi$ ).

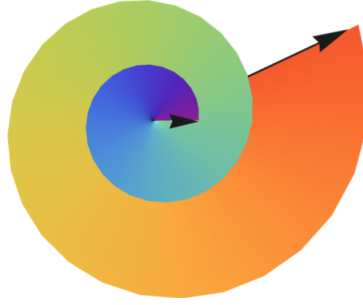


Figure 17: The projected area for two consecutive cycles in a supercritical deformation of a logarithmic spiral [schematic]. The precession per cycle  $2.125\pi$  exceeds  $2\pi$ . As the spiral develops,  $X_\perp$  sweeps out a multiply-covered region. Its progress has been color-coded using the visible spectrum. This area is proportional to  $\rho^2$ .

## 8.1 An Integral Identity

Before moving on, the reader's attention is drawn to an intriguing consequence of the identity Eq.(73), connecting the distance from the apex to the integrated trajectory history. Integrating Eq.(73) implies the identity

$$S \rho^2 = 2 \int d\mathbf{X} \cdot \mathbf{X} \times \mathbf{M} = 2\mathbf{M} \cdot \int d\mathbf{X} \times \mathbf{X}, \quad (81)$$

equating the current value of  $\rho^2$  with the area swept-out by  $X_\perp$  along the entire previous trajectory, with proportionality  $m$ . This identity is represented schematically in Figure 17. Curiously, Eq.(81) completely characterizes a planar logarithmic spiral with  $4MS = 1$  and  $\mathbf{M}$  orthogonal to the plane [11]. It also provides a new geometrical interpretation of the logarithmic trajectory in terms of its history.

## 9 Scaling and Self-Similarity

Unlike  $\phi$ , the behavior of the dimensional variables  $\rho$ ,  $X_\parallel$ , and  $X_\perp$  depend explicitly on  $\kappa = \Theta'$ . The ratio between the magnitudes of successive cycles is determined by Eq.(32):  $\kappa(2\Theta_0)/\kappa(0) = (\kappa(\Theta_0)/\kappa(0))^2 = \kappa_0^2$ . The second half of the cycle is dilated by a factor of  $\kappa_0$  with respect to the first. The growth rate, like the precession, is not uniform within the cycle itself. If  $\kappa_0$  is small (or significantly less than one) the spiral will undergo significant inflation within a single cycle. This behavior is illustrated in Figure 18 where  $\kappa_0^2$  is plotted as a function of  $m$ .

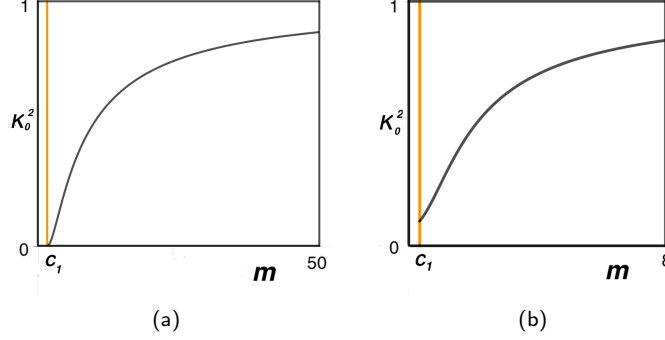


Figure 18: (a)  $\kappa_0^2$  vs.  $m$  for  $\gamma = \sqrt{2}$ . Above  $\gamma = 0.979$  ( $m = 0.9683$ ),  $\kappa_0$  rises monotonically from 0 on  $\mathcal{C}_1$ , coasting very slowly towards the asymptotic value 1 at large  $m$ . The dilation factor ( $\kappa_0^{-2}$ ) is large unless  $m$  is large, as can be appreciated by noting the range of  $m$  in the figure. When  $m$  is large  $\kappa_0 \approx 1$  and the scaling on successive cycles is modest. The vanishing of  $\kappa_0$  along  $\mathcal{C}_1$  for  $\gamma > 1$  reflects the fact that  $\Theta_0$  diverges there so that the exponential defining  $\kappa_0$  does too;  $Z$  executes one round trip in the well over the full spiral trajectory. The behavior just below  $\gamma = 1$  is anomalous in that even before  $\gamma = 1$  is reached the dilation diverges on  $\mathcal{C}_1$ . Below the value  $\gamma = 0.979$ , as illustrated in Figure 18 (b) for  $\gamma = 0.5$ ,  $\kappa_0$  does not vanish on  $\mathcal{C}_1$ . As  $\gamma$  is lowered towards zero, its initial value tends towards the limiting value 1.

The cyclic behavior of  $\kappa\rho$ ,  $\kappa X_{\parallel}$  and  $\kappa X_{\perp}$ , captured by Eqs.(45), (39) and (46), implies that

$$\rho(\Theta + \Theta_0)/\rho(\Theta) = -X_{\parallel}(\Theta + \Theta_0)/X_{\parallel}(\Theta) = X_{\perp}(\Theta + \Theta_0)/X_{\perp}(\Theta) = \kappa_0^{-1}. \quad (82)$$

The three ratios coincide. Note in particular, that the zeros of  $X_{\parallel}$  are periodic in  $\Theta$ . As a consequence the amplitudes increase exponentially with  $\Theta$ . In contrast, the cyclic variable  $\cos \theta$  is periodic with period  $2\Theta_0$ :

$$\cos \theta(\Theta + \Theta_0) = -\cos \theta(\Theta). \quad (83)$$

The dimensionless variables  $\rho'$ ,  $X'_{\parallel}$  and  $X'_{\perp}$  also form cycles (a happy accident of conformal symmetry) with periods  $\Theta_0$ ,  $2\Theta_0$  and  $\Theta_0$  respectively. In particular, the extrema of  $X_{\parallel}$  occur periodically in  $\Theta$ . Eq.(82) implies that the ratio in the magnitudes of successive extrema is given by  $1/\kappa_0$ . Note that, had  $X'_{\parallel}$  not formed a cycle, the extrema need not have occurred at  $n\Theta_0$ . For, whereas the zeros of an oscillating function are preserved under modulation, its extrema generally are not.

The second half-cycle is evidently identical to the first half, reflected in the mid-plane (switching  $\tau$  and  $-\tau$ ), rotated by  $\phi_0/2$ , and dilated by a factor of  $\kappa_0^{-1}$ . Modulo this additional symmetry, the irreducible spiral unit is described by a half-cycle.

The existence of the internal structure captured by cycles implies a significant distinction between the self-similarity in logarithmic spirals and that exhibited in their three-dimensional counterparts. Logarithmic spirals are invariant under scaling composed with an appropriate compensating rotation; if scaled appropriately, the spiral maps onto itself without rotation. Every point on a logarithmic spiral is equivalent to every other point. In their spatial counterparts, the internal structure quantizes the possible scaling so that the invariant subgroup is discrete. The spiral is invariant under scaling by the discrete factor  $\kappa_0^{-1}$ , where  $n$  is an integer, composed with a reflection in the mid plane and a rotation by  $\phi_0/2$ . This quantization reflects the additional structure of three-dimensional spirals lacking in the logarithmic prototype.

## 10 Translating cycles into spatial trajectories

To conclude, three representative supercritical trajectories will be traced to summarize what has been learned. Each of the three highlights a specific aspect of the supercritical geometry:

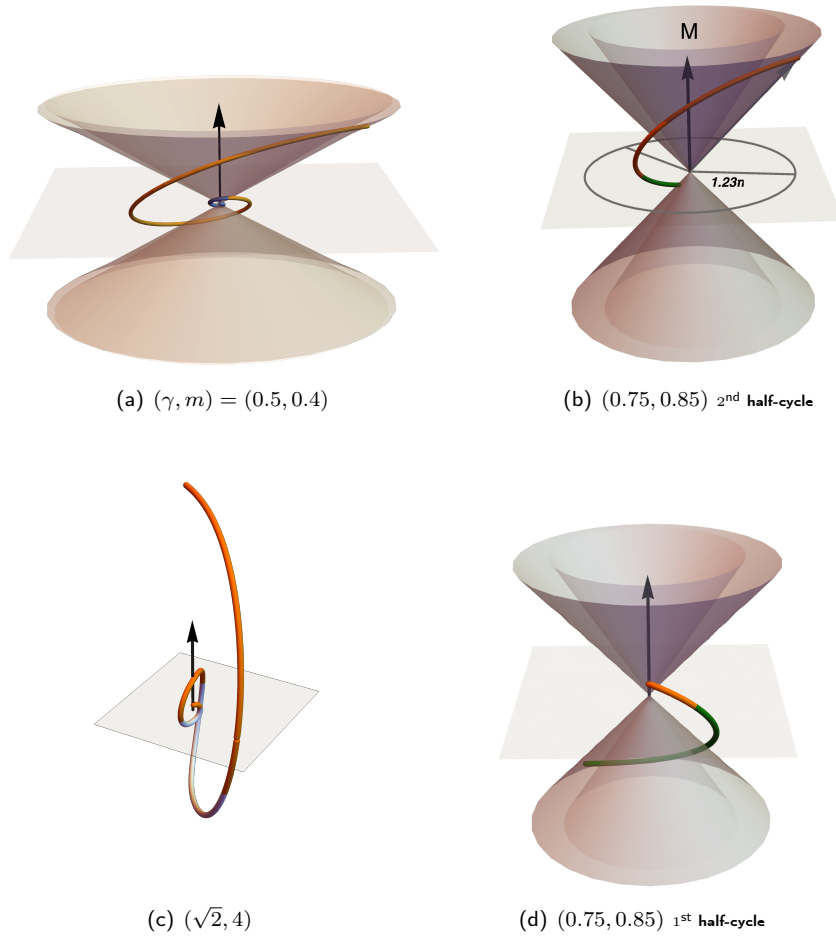


Figure 19: (a) Two consecutive cycles (blue, orange); (b,d) together represent one complete cycle of (b) (green below mid-plane, orange above) Panels (b) and (d) are in register, and (d) is scaled by a factor of 6.18 with respect to (b); (c) Single cycle (light blue below mid plane; orange above)

(a)  $\gamma = 0.5$ , and  $m = 0.4$  represents a modest deformation of a logarithmic spiral in the regime where the transition is continuous;  
(b)  $\gamma = 0.75$ ,  $m = 0.85$  represents a deformation in the same regime as (a) but with sufficient torque to resolve the invariant cones visually;  
(c)  $\gamma = \sqrt{2}$ ,  $m = 4$  represents a spiral that is not related to a logarithmic spiral by a continuous increase of  $m$  for fixed  $\gamma$  (there is, of course, a continuous path connecting it to a logarithmic spiral with  $\gamma < 1$  if  $\gamma$  is let vary); here  $\gamma > 1$  and  $m^2/\gamma^3$  is sufficiently large to reveal dramatic behavior.

#### Bounding and turning cones:

The spirals are bounded by the cones with polar angle  $\theta_{\text{Min}}$  at the apex and turn along the  $\mathbf{M}$  axis when the polar angle is  $\theta_\gamma$ :

- (a)  $\theta_{\text{Min}} = 58.22^\circ$ ,  $\theta_\gamma = 60.32^\circ$
- (b)  $\theta_{\text{Min}} = 32.38^\circ$ ,  $\theta_\gamma = 42.67^\circ$
- (c)  $\theta_{\text{Min}} < 5^\circ$ ,  $\theta_\gamma = 6.43^\circ$

The three spirals have been traced over one or more cycles in Figure 19.

Observations:

In case (a), even though the angles themselves are large, they differ only by  $2^0$ , so that two cones are just about resolved (cf. Figure 19 (a)). This reflects the sensitivity of the Cosine cycle on the value of  $m$  in this region of parameter space; the lower bound on  $m$  for this same value of  $\gamma$ , with  $\theta_{\text{Min}} = \pi/2 = \theta_\gamma$  is  $m = 0.35$ .

While the spiral trajectory along a cycle is approximately planar, this plane is not orthogonal to  $\mathbf{M}$ . The plane will itself precess in succeeding cycles as illustrated in Figure 20 (a). Here, the scaling within a cycle is by a relatively large factor ( $\kappa_0^{-2} = 9.94$ ) which explains the diminutive first cycle in Figure 19 (a).

In case (b) the spiral trajectory along a single cycle is split over two panels, scaled but in register: (b) and (d) representing the second and first half-cycles respectively. It turns out that the expansion factor is always large when the cones are well-resolved (here  $\kappa_0^{-2} = 38.15$ ). The second half-cycle is thus magnified by a factor ( $\kappa_0^{-1} = 6.18$ ) with respect to the first. Panel (d) has thus been scaled with respect to panel (b) by this factor. On closer examination the two panels are revealed to be identical modulo reflection in the mid-plane, and rotation by  $1.226\pi$ . The asymmetry between entry and exit of the return cone  $\theta_\gamma$  is evident.  $X_{\parallel}$  achieves its local extrema on exit in a growing spiral.

In case (c) the two conical polar angles are very small. For this reason, the cones have not been represented in Figure 19 (c). Even with this modest value  $m = 4$ , the two cones are essentially closed. The spiral becomes free to explore all radial directions. In Figure 19 (c), the trajectory is followed along two consecutive cycles. Surprisingly the trajectory along a single cycle does not appear, on first sight, to differ qualitatively from that displayed in (a). The two lie approximately within a plane. The difference is that this plane is rotated significantly towards the vertical in (c). This is then reflected in the patterns of precession of the nutating spirals in the two which are very different even if the angles of precession themselves are similar (cf. Figure 20).

The torque axis is indicated by the vertical black arrows in Figure 19. All three trajectories advance anti-clockwise. The torque in all three cases changes mid cycle. In (b) the angle rotated in a half cycle,  $\phi_0/2 = 221^0$  is indicated.

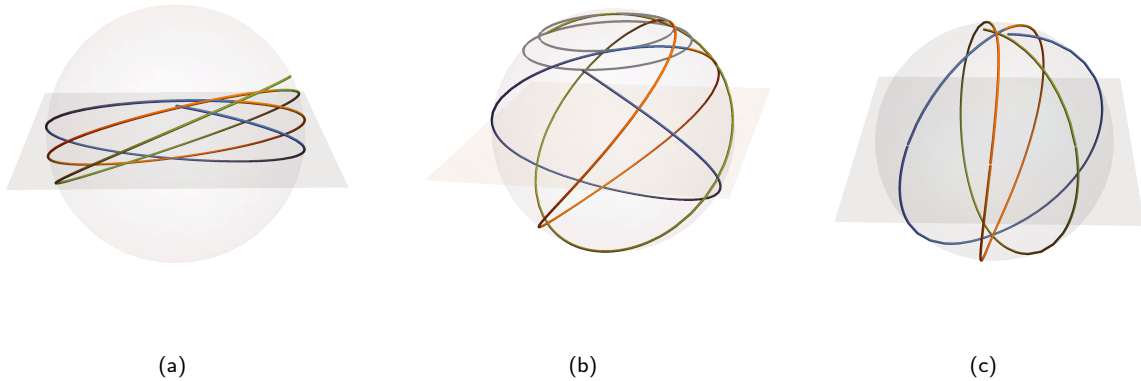


Figure 20: Three consecutive cycles (blue, yellow, green) projected onto a sphere in each of the three cases (a)-(c): the cycles are bounded between the polar angles  $\theta_{\text{Min}}$  and  $\pi - \theta_{\text{Min}}$ , the range increases as one proceeds from case (a) to (c) (with increasing values of  $m$ ). Consecutive cycles precess about the  $\mathbf{M}$  axis. The precession angle is not itself sensitively dependent on  $m$ . In case (a)  $\phi_0/(2\pi) = 1.07$ ; (2)  $\phi_0/(2\pi) = 1.23$ ; (3)  $\phi_0/(2\pi) = 1.12$ ; in all three  $\phi_0 > 2\pi$ , but otherwise the values are comparable. The different patterns exhibited in the three is, in large part, attributable to the decreasing value of  $\theta_{\text{Min}}$  as one moves from left to right. It was remarked that the individual cycles of type (a) and (c) appear superficially similar; however, it is clear here that, in the pattern of their precession, they behave very differently. In a logarithmic spiral the projection is represented by a horizontal equatorial curve. In a small deformation about a logarithmic spiral the projection will undergo small oscillations about this curve (cf. (a)). The higher value of  $\phi_0$  in the intermediate case (b) is responsible for the rapid azimuthal sweep of radial directions. In this case, the circles of constant  $\theta_{\text{Min}}$  and  $\theta_\gamma$  are traced explicitly in the northern hemisphere to facilitate the *reading* of a planar representation of the spherical projection.

To appreciate the cumulative effect of precession it is useful to follow the spiral trajectory over a number of cycles. This information is captured by the projection of the growing spiral onto a unit sphere centered at its apex, illustrated in Figure 20 for three consecutive cycles.

In cases (a) and (b), the projection orthogonal to  $\mathbf{M}$  of the cycle appears to assume the logarithmic form. This conceals the fact that  $X_{\perp}$  is not even monotonic in case (2) as revealed in Figure 21. In case (c), the orthogonal projection looks nothing like a logarithmic spiral. Thus, while superficially the spiral does appear to resemble a perturbation of the logarithmic form with respect to an almost vertical plane over a single cycle, its precession is very different in cases in cases (a) and (b).

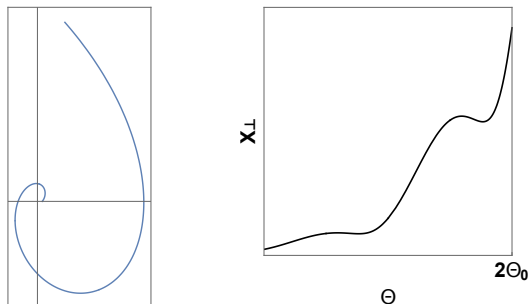


Figure 21: (L) The projection of the cycle onto the mid-plane is log spiral-like in case (b), but (R) if one examines  $X_{\perp}$  as a function of  $\Theta$  it displays significant departures from monotonicity.

Even though  $\theta_{\text{Min}} \neq 0$ , so long as it differs from  $\pi/2$ , the supercritical trajectory will eventually intersect every plane in three-dimensional space as it expands. It would appear to do this most *efficiently* when  $\theta_{\text{Min}}$  is small or the torque is large. This is analogous to the behavior of a planar logarithmic spiral, intersecting every line on the plane. In this sense, as was claimed in the introduction, supercritical spirals can be thought of as the legitimate three-dimensional analogues of logarithmic spirals.

## 11 Where we stand

The three-dimensional analogues of logarithmic spirals have been identified as the tension-free stationary states of the conformal arc length. This identification has been used to provide an explicit construction of these spirals.

This construction involves examining the three remaining conserved currents when the tension vanishes, the torque, the scaling and the special conformal currents. The tension introduces a length scale, indeed the only length scale in the problem. It is not a conformal invariant. When it vanishes, it breaks the conformal symmetry; the resulting equilibrium states are the self-similar spirals constructed here. Significantly, the conserved scaling current and the torque become translationally invariant when the tension vanishes. We have shown that if the spiral apex is located at the origin, the special conformal current vanishes. As such, self-similar spirals are characterized by just two parameters, the scaling rate  $S$  and the torque modulus,  $M$ . For conformal arc length the conserved scaling current fixes the torsion in terms of the local curvature; the conserved torque establishes the axis about which the spiral trajectory develops; its magnitude provides a quadrature determining the curvature. The vanishing conformal current is then enlisted to complete the blueprint for the construction of the spiral geometry in a polar coordinate system adapted to the spiral apex and the torque axis. In general, the determination of the torsion and curvature do not uncouple in the simple way that we have exploited. The broad outline nonetheless does appear to be independent of the specific conformally invariant energy.

On a plane, the parameters  $M$  and  $S$  are not independent. They are constrained by the relationship  $4MS = 1$ ; logarithmic spirals are characterized by a single parameter. In three-dimensions, planar spirals find themselves perched at the interface between qualitatively very different behavior depending on the value of  $4MS$ .

A planar logarithmic spiral does not exhibit any internal structure. Its three-dimensional counterparts do. Each self-similar spiral is characterized by an irreducible unit or cycle. This cycle describes nutation between two fixed coaxial circular cones with a common apex, aligned along the torque axis. The nutating pattern precesses about this axis as the spiral expands.

In subcritical spirals, with  $4MS < 1$ , the two bounding cones are oriented in the same direction. The nutating spiral forms a deformed helix that expands monotonically as it rises along the torque axis. If  $M$  is decreased to its lower bound:  $M^2 + S^2 = 1/2$ , the two cones coalesce, leaving a simple helical spiral wound about a single cone.

In supercritical spirals with  $4MS > 1$ , on the other hand, the two cones are identical but oppositely oriented (picture a *light cone*); the spiral nutates between these two cones, the region within the cone is excluded. As  $M$  increases, however, the cones close so that the spiral ranges increasingly freely through its spatial environment. As conjectured in the introduction, the trajectory followed by the circumnutating tip of a growing tendril in a climbing plant is likely to be well approximated by a supercritical template.

The behavior on crossing the interface  $4MS = 1$  in parameter space is not generally continuous. The continuous supercritical deformation of a planar logarithmic spiral by raising  $M$ , keeping  $S$  fixed requires  $2S > 1$ . One would thus expect spiral formations that can be modeled as small non-planar deviations about the logarithmic form to sit in this region of parameter space. If  $2S < 1$ , a small change in  $M$ —either up or down—results in a discontinuous change in the spiral morphology. In this context, it may be relevant that the circumnutating trajectory of a plant tendril is not a small deformation of a planar spiral.

Whereas there is a perturbative window permitting the deformation of logarithmic spirals in the supercritical direction, there are no such deformations into subcritical *helical* spirals. As  $M$  approaches its logarithmic value from below, the outer bounding cone splays out into a plane, but the inner cone does not. As a consequence, the helix tends towards the planar logarithmic form asymptotically but is not logarithmic at its center; the height of the deformed helix above the asymptotic plane is technically always infinite. It is tempting to suggest that this coincidence may be related to the absence of almost planar (as distinct from planar) spiral morphologies in mollusk shells.

Evidently, the logarithmic spiral with  $S = 1/2$ ,  $M = 1/2$  sits at the interface between very different three-dimensional spiral types in this taxonomy. Why this particular spiral and not another is not clear (it is *not* the golden ratio that crops up in plant phyllotaxis). A guess is that the conformal curvature, defined by (cf. [8, 9])

$$\mathcal{K} = -\mu(\partial_s^2 + \kappa^2/2)\mu + (\mu')^2/2, \quad (84)$$

where  $\mu$  is given by (7), vanishes in self-similar curves if and only if  $M$  and  $S$  are individually tuned to these values.

Matching a self-similar spiral to a template drawn from this minimum model involves fixing just two parameters. Any two independent measures of the geometry should be sufficient to do this, for example, the angle of nutation and the rate of precession, both captured in Figure 20. A third measure (say the expansion rate) had better be consistent with the first two. Significant deviations could, however, be pointing to additional structure.

One way additional internal structures will occur is if higher order conformal invariants or constraints are relevant. As an example of the former, the conformally invariant bending energy,  $H = \int ds \mathcal{K}^2 (\kappa'^2 + \kappa^2 \tau^2)^{1/2}$ , constructed using the conformal curvature (84) would be expected to exhibit more complex three-dimensional self-similar spirals. The planar reduction of this problem exhibits non-logarithmic spirals as equilibrium self-similar structures. In the spirit of the Euler-Elastic analogue [20], placing a constraint on the total torsion (a conformal invariant modulo  $2\pi$ ) adds an additional twist to the problem.

## Acknowledgments

I have benefitted from discussions with John Guven and Denjoe O' Connor. Gregorio Manrique's assistance with Mathematica is very much appreciated. I also thank Niloufar Abtahi for her careful reading of the manuscript as well as for removing gratuitous daylight between words. Partial support from (the now expired) CONACyT grant no. 180901 is acknowledged.

## Appendix A Logarithmic helices and curves with $|\mathbf{X}| = \alpha s$

Let  $s \rightarrow \mathbf{X}$  describe a space curve such that  $|\mathbf{X}|^2 = \alpha^2 s^2$ ,  $0 \leq \alpha \leq 1$ . On a plane, this is necessarily a logarithmic spiral. In space, it allows considerably greater freedom.

In general,

$$\mathbf{t} \cdot \mathbf{X} = \alpha^2 s, \quad (\text{A.1})$$

or equivalently,  $\mathbf{t} \cdot \hat{\mathbf{X}} = \alpha$ , so that the tangent vector again makes a constant angle with the radial vector (with cosine given by  $\alpha$ ). Differentiating again, one finds

$$1 - \kappa \mathbf{n} \cdot \mathbf{X} = \alpha^2. \quad (\text{A.2})$$

In three dimensions, this identity is differentiated once again to produce the homogeneous relationship between the three projections:

$$-\kappa' (\mathbf{n} \cdot \mathbf{X}) - \kappa^2 (\mathbf{t} \cdot \mathbf{X}) + \kappa \tau (\mathbf{B} \cdot \mathbf{X}) = 0. \quad (\text{A.3})$$

Using the completeness of  $\mathbf{t}$ ,  $\mathbf{N}$  and  $\mathbf{B}$  to equate  $|\mathbf{X}|^2$  with the sum of the squares of its projections, given by Eqs.(A.1), (A.2) and (A.3), the constraint on  $\kappa$  and  $\tau$ ,

$$\alpha^2 (1 - \alpha^2) s^2 = (1 - \alpha^2)^2 \frac{1}{\kappa^2} + \left( \frac{\kappa'}{\kappa^2 \tau} (1 - \alpha^2) + \frac{\kappa}{\tau} \alpha^2 s \right)^2, \quad (\text{A.4})$$

is identified. On a plane, this reduces to  $\kappa s = \sqrt{(1 - \alpha^2)/\alpha^2}$ . This relates the scaling current to  $\alpha$  in a planar equilibrium:  $\alpha = \arctan 2S$ .

Introducing  $\Sigma$  and  $\Gamma$  defined by Eqs.(12), the constraint can be rephrased as

$$(c_0^2 \kappa^2 s^2 - 1) \Gamma^2 = (\Sigma - c_0^2 \kappa s)^2, \quad (\text{A.5})$$

where  $c_0^2 = \alpha^2 / (1 - \alpha^2)$ . Suppose that  $c \kappa s = 1$ , where  $c$  is a constant. Then  $\Sigma = c$ , and Eq.(A.5) implies  $\Gamma^2 = c_0^2 - c^2$ . Thus if  $c \neq c_0$ ,  $[c^2 / (c_0^2 - c^2)]^{1/2} \tau s = 1$ ;  $\tau$  vanishes if  $c = c_0$ , reproducing the planar result. These are helical spirals; Notice that as  $\alpha$  ranges from 0 to 1,  $c_0$  ranges from 0 to  $\infty$ . Thus all possible helical spirals are consistent with the equation,  $|\mathbf{X}| = \alpha s$ . There is no bound placed either on  $\tau/\kappa$  or  $\kappa$ .

Now examine the conical helical tension-free states with constant  $\Sigma$  and  $\Gamma$ . The quadrature (23) implies that  $\Sigma$  is constant only if the parameters  $M$  and  $S$  are fine-tuned so that a double root occurs. This requires  $2S \leq 1$ . Then  $\Sigma = 2S$  so that  $2S \kappa s = 1$ . Eq.(13) then implies that  $\Gamma = \sqrt{1 - (2S)^2}$ . Thus there is an upper bound on  $\tau/\kappa$  and a lower bound on  $\kappa s$ . Substituting these results into Eq.(A.5) implies the constraint

$$(c_0^2 - (2S)^2) (1 - (2S)^2) = ((2S)^2 - c_0^2)^2. \quad (\text{A.6})$$

The only solution is  $c_0 = 1$ , so that  $\alpha^2 = 1/2$ .

There are, of course, other curves that are consistent with Eq.(A.5). Indeed, given  $\Gamma$ , then the constraint determines  $\Sigma$ . The equation can then be integrated to give  $\kappa$  and thus  $\tau$  using the functional form of  $\Gamma$ .

## Appendix B Tension-free Conical Helices

Before looking at spiral trajectories in complete generality, it is instructive to examine conical helices in the light of the geometrical identities now in our possession. Conical helices arise when the two roots of the quadratic appearing in the potential (24) coincide. As seen below Eq.(28), this occurs when  $Z = \gamma^{-1/2}$  and  $\gamma \geq 1$  (or  $\Sigma = 2S$  and  $2S \leq 1$ ). This equation can be integrated to give

$$\kappa s = (2S)^{-1}. \quad (\text{B.1})$$

Eq.(13) now implies that the ratio  $\tau/\kappa$  is also constant;  $\tau/\kappa = \sqrt{1 - (2S)^2}$ . Using Eq.(B.1), this implies

$$\tau s = \sqrt{1 - (2S)^2} / (2S). \quad (\text{B.2})$$

To construct the spiral trajectory, note that  $Q$ , defined by Eq.(41), vanishes so that Eq.(45) reduces to

$$(1 + m^2)\kappa^2\rho^2 = [\gamma^2(\gamma - Z_0) + \gamma Z_0^{-1}], \quad (\text{B.3})$$

where  $Z_0 = \gamma^{-1/2}$ . Using the identity (28), and Eq.(B.1), the distance to the apex is found to be  $\rho = s/\sqrt{2}$ . Unlike the curvature or torsion  $\kappa$  and  $\tau$ , this is independent of the value of  $S$ . As will be seen, if  $m$  is raised keeping  $S$  fixed, the spiral will nutate and  $\rho$  grows sublinearly with  $s$ .

These tension-free helices lie on a cone with a constant opening angle. The cosine of this angle, determined by Eq.(47), is given by

$$\cos \theta_0 = \sqrt{\frac{1 - (2S)^2}{1 - 2S^2}}; \quad (\text{B.4})$$

its sine has a very simple expression in terms of  $m$ :

$$\sin \theta_0 = \frac{\sqrt{2}S}{\sqrt{1 - 2S^2}} = \frac{1}{m}. \quad (\text{B.5})$$

The vertical rise  $X_{\parallel} = \rho \cos \theta_0$  is completely determined by  $\theta_0$ ,  $X_{\parallel}(s) = s \cos \theta_0 / \sqrt{2}$ . When  $2S = 1$ ,  $\theta_0 = \pi/2$  so that the cone splays open into a plane and the conical helix coincides with a planar logarithmic spiral.

We note that cones with a fixed  $\theta_0$  are preserved under conformal inversions centered on the apex. One can further confirm that, modulo the reversal of torsion, the spiral on this cone is as well. Conical helices corresponding to distinct value of  $S$  (or  $\theta_0$ ), are conformally inequivalent.

The projection on the plane (described by the cylindrical polar  $X_{\perp} = \rho \sin \theta_0$ ) is also a logarithmic spiral:  $X_{\perp} = s \sin \theta_0 / \sqrt{2} = s/(m\sqrt{2})$ . Thus the parameter  $\alpha$  defined in Appendix A is given by  $\alpha = 1/(m\sqrt{2})$ , with a maximum  $\alpha = 1/\sqrt{2}$  occurring when  $\theta_0 = \pi/2$ . Not all logarithmic spirals are realized by projection.

In a conical helix,  $\rho'^2 + \rho^2 \sin^2 \theta_0 \phi'^2 = 1$ . Thus  $s^2 \sin^2 \theta_0 \phi'^2 = 1$ , or

$$\phi = \ln s / \sin \theta_0. \quad (\text{B.6})$$

An interesting corollary is that the conical pitch (or the angle  $\Phi$  that the tangent makes with circles of constant  $\rho$ ) is constant, given by  $\tan \Phi = \rho'/(X_{\perp} \phi') = 1$ , or  $\Phi = \pi/4$  independent of  $\theta_0$ . This should not be conflated with the angle that the tangent makes with the torque axis, introduced in Eq.(42), which is also constant, but  $\theta_0$  dependent, given now by  $\cos \Psi = X_{\parallel}' = \cos \theta_0 / \sqrt{2}$ .

To summarize, there is a one-to-one correspondence between cones and the tension-free spirals they host. But key properties—notably the distance–arc length relationship and the pitch—turn out to be independent even of this cone.

### Period of small oscillations about conical helices

The curvature of the potential (24) at  $Z = \gamma^{-1/2}$  determines the period of small oscillations about a conical helix. The harmonic approximation gives

$$Z^{\bullet\bullet} + 4(1 - \gamma^{-3/2})(Z - \gamma^{-1/2}) \approx 0, \quad (\text{B.7})$$

so that this period is given by  $\Theta_0 = 2\pi/\omega$ , where  $\omega = 2\sqrt{1 - \gamma^{-3/2}} = 2\sqrt{1 - 4S^2}$ . We are now in a position to express  $\phi$  as a function of  $\Theta$ . The relationship  $\kappa s = (2S)^{-1}$  implies, upon integration, that  $\Theta = \ln s / 2S$ . Together with the identity Eq.(B.6), it follows that

$$\phi = \sqrt{2}\sqrt{1 - 2S^2} \Theta, \quad (\text{B.8})$$

so  $\phi$  is proportional to  $\Theta$  in conical spirals; the two diverge with a ratio of 1 as  $2S \rightarrow 1$  (or  $\gamma \rightarrow 1$ ). Importantly,  $\phi$  always exceeds  $\Theta$ ; this property will be seen to hold in all tension-free states and will provides an important pointer towards an understanding of their global geometry. In one period  $\Theta_0$ ,  $\phi$  rotates by the angle



$\phi_0 = \sqrt{2\pi} \sqrt{(1-2S^2)/(1-4S^2)}$ , increasing monotonically with  $S$ . Below  $S = 1/\sqrt{6}$  (or  $\theta_0 < \pi/4$ ),  $\phi_0 < 2\pi$ ; above it,  $\phi_0 > 2\pi$  (diverging as  $2S \rightarrow 1$  because  $\Theta_0$  does).  $\phi_0 = 2\pi$  occurs where  $\tau/\kappa$  is maximized. In supercritical spirals it will be seen that  $\phi_0$  always exceeds  $2\pi$ .

We are also in a position to determine the decline in curvature over a given period either of  $\Theta$  or a revolution about the axis. We have, using Eq.(31),

$$\kappa_0 := \frac{\kappa(\Theta_0)}{\kappa(0)} = e^{-\gamma^{-3/2}\Theta_0} = \exp\left(-\pi\sqrt{\frac{4S^2}{1-4S^2}}\right) = \exp\left(-\sqrt{2}\pi \tan \theta_0\right), \quad (\text{B.9})$$

where the identity  $Z_0 = \gamma^{-1/2} = (2S)^{2/3}$  has been used in the first expression, the expression for  $\Theta_0$  given below Eq.(B.7) in the second, and the trigonometric identities (B.4) and (B.5) in the third. As  $2S \rightarrow 1$ ,  $\theta$  opens and  $\kappa_0 \rightarrow 0$ . In this limit, there is no oscillation so that  $\Theta_0$  ceases to represent a useful measure of the geometry. The identity does suggest that the dilation per period is largest near the critical point  $2S = 1$ ,  $2M = 1$ . This is generally true.

## Appendix C Derivation of Eq.(52)

$$\begin{aligned} W_{\pm}^{\bullet} &= \left( (Z - Z_-)^{-1/2}(Z_+ - Z)^{1/2} - (Z - Z_-)^{1/2}(Z_+ - Z)^{-1/2} \right. \\ &\quad \left. \pm [Z^{-1/2}(\gamma - Z)^{1/2} - Z^{1/2}(\gamma - Z)^{-1/2}] \right) Z^{3/2}Q(\gamma - Z) \\ &= [(m^2 + 1)/\gamma^2 - 2Z]Z(\gamma - Z)^{1/2} \pm [\gamma - 2Z]Z^{1/2}Q. \end{aligned} \quad (\text{C.1})$$

Thus, at an extremum,  $Q$  is given by

$$Q = \mp \left( \frac{(m^2 + 1)/\gamma^2 - 2Z}{\gamma - 2Z} \right) Z^{1/2}(\gamma - Z)^{1/2}, \quad (\text{C.2})$$

or, equivalently,

$$Z(\gamma - Z) \left( \frac{m^2 + 1}{\gamma^2} - 2Z \right)^2 + \left( Z^2 - \frac{m^2 + 1}{\gamma^2} Z + \frac{1}{\gamma} \right) (\gamma - 2Z)^2 = 0, \quad (\text{C.3})$$

which, despite appearances, reduces to the vanishing of the quadratic in  $Z$  give by (52).

## Appendix D Sharp upper and lower bounds on $\rho'$

It is straightforward to confirm that  $\rho' \leq 1$  which, in turn, implies  $\rho \leq s$ .

### Supercritical vs. Subcritical spirals

In a supercritical spiral,  $W_- = -Q + Z^{1/2}(\gamma - Z)^{1/2} = 0$  when  $Z$  satisfies Eq.(50), the necessary criterion that  $\cos \theta = 0$  discussed in section 5. This locates the maximum  $\rho'$  at mid-plane-crossing.

In a subcritical spiral, there is a non-vanishing minimum value of  $\cos \theta$  which places a sharp upper bound on  $\rho'$ . It was seen that this occurs where  $W_-^{\bullet} = 0$ , which is determined by the quadratic appearing in Eq.(52).

In summary

$$\rho'^2 \leq \begin{cases} \frac{\gamma^3}{m^2+1} \leq \frac{\gamma^3}{\gamma^3+1}, & m^2 \geq \gamma^3; \\ \frac{\gamma^3}{m^2+1} \frac{1}{1+\gamma W_-(Z_0)^2} \leq \frac{m^2}{m^2+1}, & m^2 \leq \gamma^3. \end{cases} \quad (\text{D.1})$$

It is possible to also place sharp lower bounds on  $\rho'$  by determining the maxima of  $|W_+|$ . A weaker bound on  $\rho'$  follows from the trigonometric bound,  $|W_+|^2 \leq m^2/\gamma$ , following from the identity (77):

$$\rho'^2 \geq \frac{\gamma^4}{m^2+1} \frac{1}{m^2+\gamma}. \quad (\text{D.2})$$

## Appendix E Asymptotic rise as $m^2 \uparrow \gamma^3$

As  $m^2 \uparrow \gamma^3$ , the linear helical ascent along the torque axis of the deformed helices slows down, growing sub-linearly with  $s$  (compared to the linear growth in a conical helix). In the limit the increasingly deformed helix degenerates as  $s \rightarrow \infty$  into a planar logarithmic spiral. Let us now determine the exponent associated with this critical slowdown.

If  $Z \rightarrow \gamma$  in Eq.(39), then

$$X_{\parallel} \rightarrow S \left( \frac{1}{\kappa} \right) \left[ (1 - \gamma^{-3})^{1/2} + 1 \right] (\gamma - Z)^{1/2}. \quad (\text{E.1})$$

To determine the asymptotic behavior as  $Z \rightarrow \gamma$ , the potential is expanded about the double root at  $Z = \gamma$  in Eq.(23):

$$Z^{\bullet 2}/2 + 2\gamma^3(1 - \gamma^{-3})(\gamma - Z)^2 = 0, \quad (\text{E.2})$$

with solution

$$\gamma - Z \approx Ae^{-\Omega\Theta}, \quad (\text{E.3})$$

where  $\Omega^2 = 4\gamma^3(1 - \gamma^{-3})$ . This implies that  $\kappa \approx ce^{-\gamma^{3/2}\Theta}$ , so that  $s \approx c^{-1}\gamma^{-3/2}e^{\gamma^{3/2}\Theta}$  consistent with the asymptotic behavior as a planar logarithmic spiral,  $\kappa s \approx \gamma^{-3/2} = (2S)^2$ . Now  $\gamma - Z \approx As^{-\gamma^{-3/2}\Omega} = As^{-2\sqrt{1-\gamma^{-3}}}$ . Thus

$$X_{\parallel} \rightarrow [(1 - \gamma^{-3})^{1/2} + 1]s^{1-(1-\gamma^{-3})^{1/2}}, \quad (\text{E.4})$$

diverging sub-linearly with  $s$ .<sup>5</sup>

## Appendix F Extrema of $\tau/\kappa$

In section (3.1.2) It was shown that, whenever  $Z = Z_{\tau \max} = 2\gamma/3$  is accessible, the extrema of  $\tau$  occur there. To determine if  $Z_{\tau \max}$  is accessible, first note that  $Z_{\tau \max} \geq Z_-$ , whenever

$$m^2 - 2 \geq 2/3(\gamma^3 - 9/4), \quad (\text{F.1})$$

and  $\gamma^3 \leq 9/4$ , equality holding along a straight line with respect to the variables  $(\gamma^3, m^2)$  (cf. Figure 22). If  $\gamma^3 > 9/4$  the inequality (F.1) holds for all admissible trajectories. There is a small window of both subcritical and supercritical trajectories in which the maximum ratio occurs at  $Z_-$ .

On the other hand, note that  $Z_{\tau \max} \leq Z_+$  whenever the inequality (F.1) holds and  $\gamma^3 \geq 9/4$ . If  $\gamma^3 \leq 9/4$ , (F.1) holds for all admissible trajectories. There is no upper constraint in supercritical trajectories.

At the endpoint  $\gamma^3 = 9/4$ ,  $m^2 = 2$  where the two segments meet, the line touches the curve  $\mathcal{C}_0$  in parameter space tangentially. Recall that along  $\mathcal{C}_0$ , the two roots of the potential coincide  $Z_- = Z_+$ . Thus the conical helix with the greatest  $\tau/\kappa$  occurs when  $\gamma^3 = 9/4$  and  $m^2 = 2$ . Now  $\Gamma_{\max} = \sqrt{1 - (2S)^2} = 1/\sqrt{3}$ . This particular helix also saturates the bound (19).

## References

- [1] D.W. Thompson, *On growth and form*, (Cambridge University Press, Cambridge, England, 1942).
- [2] X. Chen, S. Wang, L. Deng, R. de Grijs, C. Liu and H. Tian *An intuitive 3D map of the Galactic warp's precession traced by classical Cepheids* Nature Astronomy, Letter 04 February (2019)
- [3] M. Pietsch, L. Aguirre Dávila, P. Erfurt, E. Avci, T. Lenarz and A. Kral *Spiral Form of the Human Cochlea Results from Spatial Constraints* Sci Rep. 2017; 7: 7500.
- [4] J.W. Milnor, *The geometry of growth and form*, Talk given at the IAS, Princeton, 2010, available at <http://www.math.sunysb.edu/~jack/gfp-print.pdf>

---

<sup>5</sup>In the limit  $\gamma \rightarrow \infty$ , the limiting value is finite.

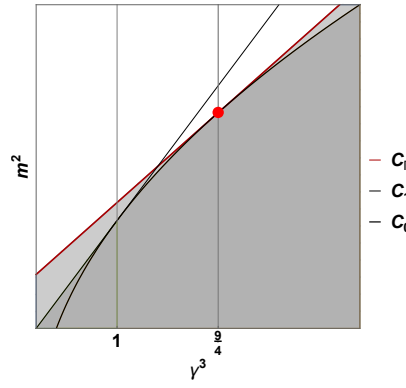


Figure 22: Above  $C_\Gamma$ ,  $\Gamma$  assumes its maximum  $2\gamma^3/(3\sqrt{3})$ ; in the gray region below  $C_\Gamma$  with  $\gamma^3 < 9/4$ ,  $Z_\Gamma < Z_-$ , the maximum is assumed at  $Z_-$ ; in the gray region below  $C_\Gamma$  with  $\gamma^3 > 9/4$ ,  $Z_\Gamma > Z_+$  and the maximum is assumed at  $Z_+$ .

- [5] J. Guven *Conformal Mechanics of Space Curves* (2019)
- [6] G. Harary and A. Tal, *The Natural 3D Spiral* Eurographics 2011, (M. Chen and O. Deussen, Guest Editors) **30** 2 (2011); *3D Euler spirals for 3D curve completion* Computational Geometry **45** 115-126 (2012)
- [7] T.J. Willmore, *Total Curvature in Riemannian Geometry* (Ellis Horwood, Chichester, 1982)
- [8] G. Cairns, R. Sharpe, and L. Webb, *Conformal invariants for curves and surfaces in three dimensional space forms*, Rocky Mountain J. Math. **24** 933-959 (1994); G. Cairns and R.W. Sharpe, *On the inversive differential geometry of plane curves*, Enseign. Math. **36** (1990), 175-196 (1990)
- [9] E. Musso, *The conformal arc-length functional* Math. Nachr. **165** 107-131 (1994)
- [10] M. Bolt *Extremal properties of logarithmic spirals* Beitrage zur Algebra und Geometrie **48** 493-520 (2007)
- [11] J. Guven and G Manrique *Conformal Mechanics of Planar Curves* (2019)
- [12] M. Do Carmo, *Differential Geometry of Curves and Surface* (Prentice Hall, Upper Saddle River, 1976)
- [13] Darwin C, Darwin F. *The power of movement in plants*. London: John Murray 1880
- [14] M. Stolarz, *Review: Circumnutation as a visible plant action and reaction* Plant Signaling & Behavior 4:5, 380-387 (2009)
- [15] Cucumber Growth Time Lapse Video [https://www.youtube.com/watch?v=voyBLb6\\_u50](https://www.youtube.com/watch?v=voyBLb6_u50) The intelligent design invoked by the poster is a tad unfortunate.
- [16] Maria Stolarz, Maciej Zuk, Elzbieta Krol, Halina Dziubinska *Circumnutation Tracker: Novel software for investigation of circumnutation* Plant Methods 10(1):24 (2014)
- [17] R. Bastien and Y. Meroz, *The Dynamics of Plant Nutation Result From the Slaving of Curvature to the Orientation of Differential Growth* PLoS Comput Biol 12(12): e1005238 (2016)
- [18] S.R. Finch and Li-Yan Zhu, *Searching for a Shoreline* <https://arxiv.org/abs/math/0501123> (revised 2016)
- [19] M. Magliaro, L. Mari, and M. Rigoli, *On the geometry of curves and conformal geodesics in the Moebius space*, Ann. Global Anal. Geom., **40** 133-165 (2011)
- [20] T. A. Ivey and D. A. Singer, *Knot types, homotopies and stability of closed elastic rods* Proc. Lond. Math. Soc. **79** 429 (1999)